Technical Note

1967-24

M. P. Fraser

Project MAPOLE

(Magnetic Dipole Spark Transmitter)

22 May 1967

Lincoln Laboratory

MASSACHUSETTS INSTITUTE OF TECHNOLOGY

Lexington, Massachusetts

MASSACHUSETTS INSTITUTE OF TECHNOLOGY

LINCOLN LABORATORY

PROJECT MAPOLE

(Magnetic Dipole Spark Transmitter)

M. P. FRASER

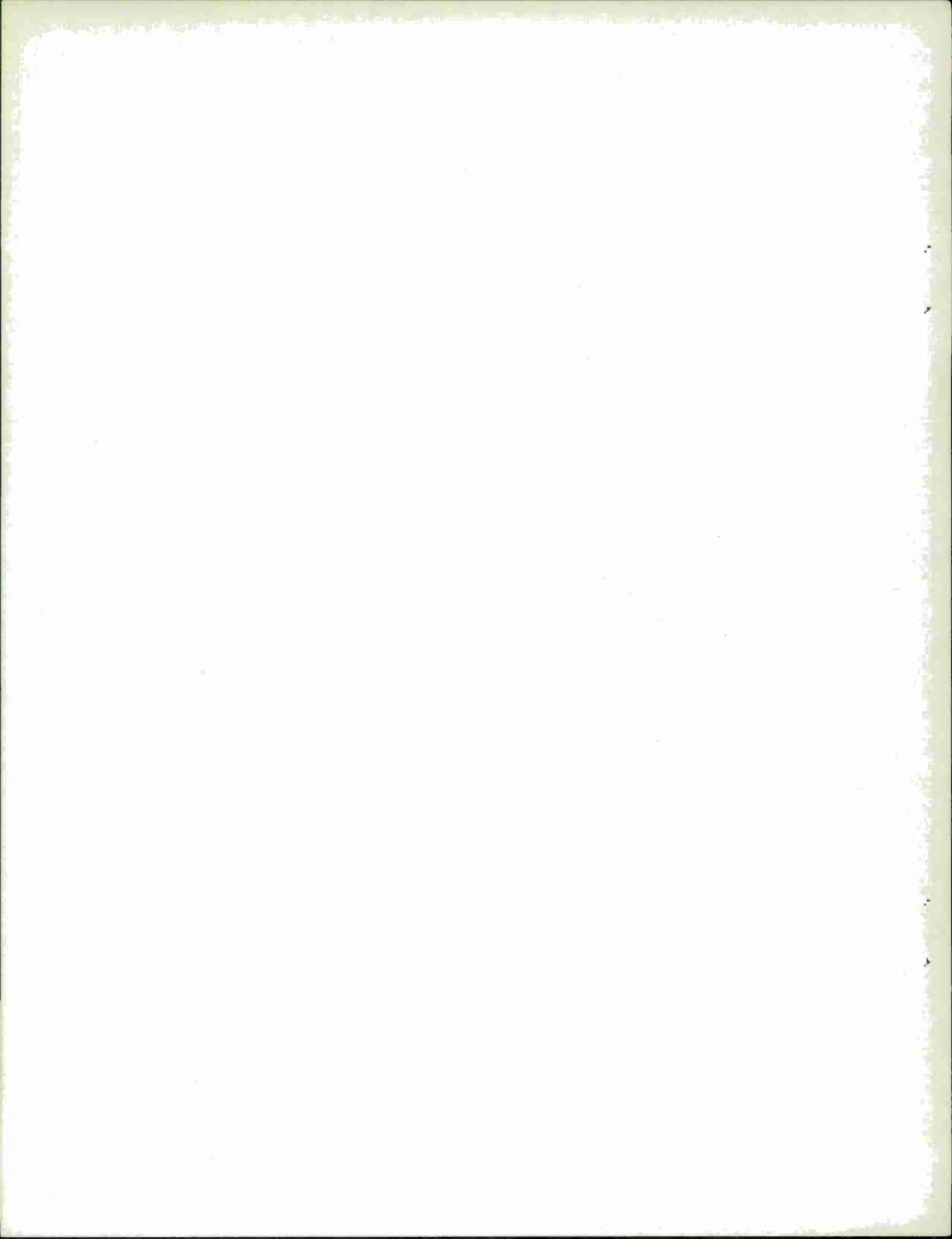*Group 43*

TECHNICAL NOTE 1967-24

22 MAY 1967

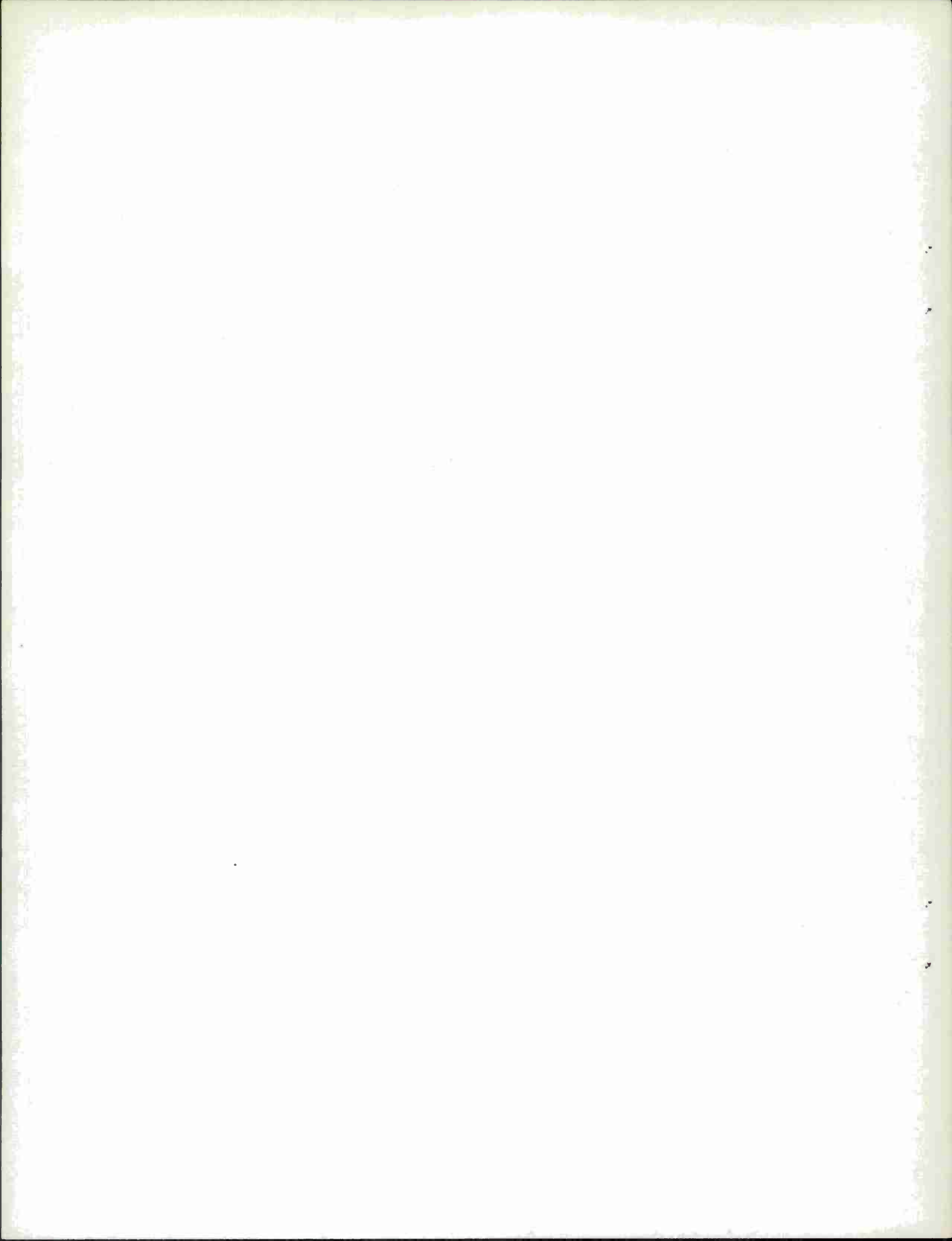LEXINGTON   MASSACHUSETTS

ABSTRACT

This report describes theoretical and experimental work on the
development of a VHF high-power closed-ring spark trans-
mitter, a device theoretically capable of producing gigawatt
peak powers in the nanosecond pulse-length region. The inves-
tigation and this report were conveniently divided into three
distinct, though interrelated, categories: First, the theoretical
aspects of transmitter performance; second, an investigation
of certain aspects of spark-gap performance germane to the
entire undertaking; finally, the construction and experimental
evaluation of the complete transmitter.

CONTENTS

PROJECT MAPOLE

(Magnetic Dipole Spark Transmitter)

SUMMARY

The feasibility of utilizing modern spark-transmitter techniques to generate high pulse power at VHF and lower frequencies was demonstrated in this program. The broad objectives of the effort covered the theoretical and experimental investigation of a VHF closed-ring spark transmitter and relevant aspects of spark-gap performance. The experimental transmitter produced 16-MW pulses of 20-ηsec duration although operating at only 1.4-percent efficiency. Further development, particularly in the area of spark-gap triggering processes, could yield transmitters capable of gigawatt peak-power operation.

Although the present investigation of spark transmitters utilized the closed-ring or magnetic dipole structure, the basic concept is not limited to this configuration. The underlying principle of operation involves capacitors, charged in parallel and discharged in series through spark gaps, resonating with associated inductances to produce oscillations. Unlike historical spark transmitters, the spark gap is used only as a convenient switch. Extensive experimental work indicates the desirability of pressurizing the spark gaps with a $90\% N_2$-$10\% CO_2$ atmosphere and utilizing high-energy triggering schemes. Proper application of the methods described in this report, particularly those that affect multiple-gap synchronization, is a prerequisite to successful transmitter operation.

I.   HISTORICAL INTRODUCTION

The original wireless spark transmitters, used at the turn of the century, produced damped oscillations by discharging a capacitor into an inductance. A decade later, CW power was generated by employing the negative resistance characteristics of the spark to overcome the losses in the LC circuit. The present investigation utilizes the spark only as a convenient switch and, as such, it could be replaced by some other suitable device having the proper characteristics. Research on modern spark transmitters was originally performed by Dr. K. Landecker and his associates at the University of New England, Australia, in the late 1950's and has been continuing there on a part-time basis.[1] Although many novel schemes of high-power spark transmission have been suggested by these workers, a practical transmitter has never been operated successfully. Stanford Research Institute has been investigating these schemes for the Advanced Research Projects Agency through the Office of Naval Research since June 1963 in an attempt to apply them to a working transmitter.[2-7] Experiments have been performed with several transmitters in the 6- to 470-MHz range. Efficiencies on the order of several percent were obtained at the lower frequencies, although negligible output power was produced at the higher

frequencies. Lincoln Laboratory initiated the investigation of spark-transmitter techniques in October 1964, concentrating on a closed-ring VHF model, the magnetic dipole transmitter.

II. BASIC TRANSMITTER THEORY

The magnetic dipole transmitter consists of a number of capacitors, placed around the circumference of a ring, which are charged in parallel through resistors and discharged in series through spark gaps, as shown in Fig. 1. The inductance of the ring, capacitors, and spark channels resonate at the operating frequency, producing damped oscillations. The device is attractive because of its simplicity (the transmitter and antenna are one and the same) and the unequaled available output power at short pulse widths. For example, at the upper VHF frequencies, theoretical peak output powers exceeding 10,000 MW at energy levels of 100 J per pulse are predicted.
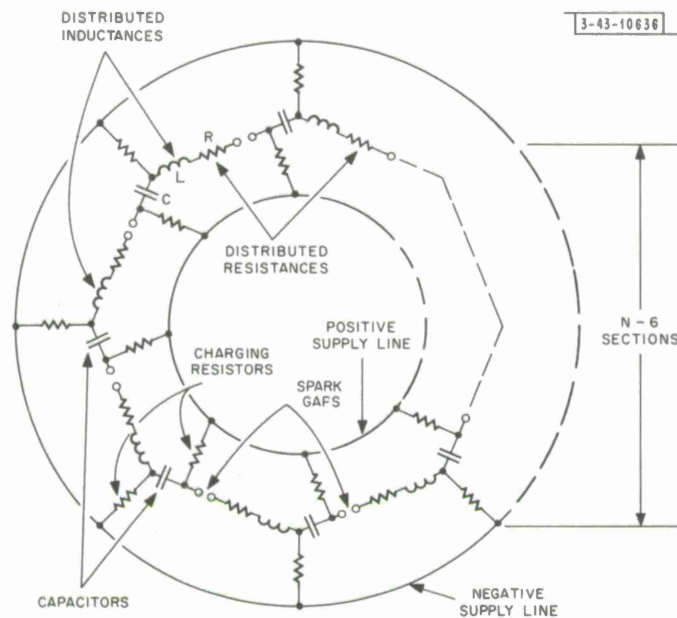
Fig. 1. Basic magnetic dipole transmitter.

This concept is not limited to the ring structure described above, but can be applied to many other configurations, the most basic being the unit oscillator. This elementary structure consists of a single capacitance-inductance pair transferring energy to a small antenna through a switch, perhaps a spark gap. Other forms include linear arrays of unit oscillators, several types of parasitically coupled circuits, as well as variations in the basic ring structure itself. Some of these schemes have been tried with little success by other workers,[1-7] but they are not symmetrical in construction and do not offer the simplicity and engineering practicality of the basic ring structure. Accordingly, the experimental vehicle to be used in this investigation of spark transmitters will be the ring-form or magnetic dipole.

A. Design Equations

The magnetic dipole transmitter essentially consists of N damped RLC circuit sections in series around the periphery of a ring. The energy stored in each capacitor C will resonate

with the inductance of each section L (consisting of terminal, capacitor, and spark-channel self- and mutual-inductances) at an angular frequency ω, and be dissipated in the total section resistance R (consisting of spark-gap and circuit losses R_L, as well as radiation resistance R_R). The circulating current, and therefore radiated energy, will be in the form of exponentially decaying waves. All the interrelated circuit parameters may be derived from the simple RLC model or obtained in the literature.[1] The circuit will possess the characteristic quality factor Q, given by

$$Q = \frac{\omega L}{R} \tag{1}$$

and, when charged to some voltage V, will store a total energy W in the capacitors (which, in the lossless case, is the energy radiated per pulse) given by

$$W = N(\frac{1}{2} CV^2) \tag{2}$$

The peak power $\hat{P}$ of the first cycle of RF available for radiation, considering the lossless case, can be expressed as

$$\hat{P} = \frac{2W\omega}{Q} \ e^{-\pi/2Q} \tag{3}$$

and the pulse length to the 10-percent power point Δt as

$$\Delta t = \frac{2.3Q}{\omega} \tag{4}$$

If the mean ring diameter is D and the free-space wavelength is λ, then the total radiation resistance R_{RT} of such a ring is

$$R_{RT} = NR_R = 20\pi^2 k^4 \left(1 - \frac{k^2}{5} + \frac{k^4}{56} - \ldots\right) \tag{5}$$

where

$$k = \frac{\pi D}{\lambda} \tag{6}$$

Equation (5) presupposes that the current flowing in the loop is equiphased at all places. This is generally true for small loops where $D \ll \lambda$. The magnetic dipole transmitter, although not a small loop, satisfies the phase criterion of Eq. (5) since a multitude of equiphased-current generators are effectively placed around the periphery of the loop.[8] The radiation will be in the plane of the loop, having the general shape of a toroid (the electric vector oscillating concentrically with the loop, the magnetic vector concentrically with a cross section of the toroid) for values of $D/\lambda < 0.585$ (Ref. 9). For larger loops, multiple lobes will be formed.

The inductance L of each section of a loop having a mean conductor diameter d can be expressed as

$$L = \frac{0.2\pi D}{N} \ (\ln \frac{8D}{d} - 2 + \mu_r \delta) \times 10^{-6} \tag{7}$$

where the units are in the mks system, and $\mu_r \delta$ is a skin-effect correction factor which can be neglected for practical values of mean conductor diameter. It is difficult to calculate the mean conductor diameter since it includes the fluctuating spark-channel diameter, the various physical conductor diameters, and the mean diameter of the current path through the capacitors.

It is at once apparent that the design parameters of any magnetic dipole transmitter are interrelated, and the only approach that will yield productive results must utilize an iterative process. A good start, after deciding on the operating frequency, is to choose different values of D/λ and with a few other assumptions calculate the remaining parameters for each of the values assumed.

B. Multiple-Gap Triggering

In order to achieve successful transmitter operation, the current generators placed around the periphery of the loop must be equiphased as stated in the previous section. This implies that all the multiple-spark gaps must break down in synchronism. Methods of effecting synchronism include overvolting the gaps or secondary trigger electrodes, and/or illuminating the gaps with laser, ultraviolet, gamma, or x-radiation, as well as direct injection of electrons. Pressurization of the gaps, and the type of fill gas used, also influence the degree of synchronization. These methods will be discussed in detail in Sec. III. Nonsynchronization in the breakdown of the multiple-spark gaps causes a redistribution of charge in the transmitter and a lack of coherence in the resultant radiation. The lack of coherent radiation is accompanied by a distortion of the expected radiation pattern, and suggests that the units comprising the transmitter are operating independently. Alternatively, if the transmitter is considered a traveling-wave structure, then modes other than the fundamental are being excited. In order to assure coherent radiation, the gaps must be synchronized within small fractions of a wave period.

The charge redistribution manifests itself as an exchange of stored energy between the internal and external capacities of the transmitter once breakdown has been initiated in some of the gaps. The externally stored energy is subsequently discharged in the form of parasitic oscillations. Stray capacity to ground will also affect the charge redistribution and set up separate parasitic oscillations with the circuit inductances. If the ratio of external and stray to internal transmitter capacity can be made extremely small, and gap breakdown is random around the periphery of the transmitter (as it is likely to be), the total energy lost by this mechanism will be small, even though gap synchronization times are larger than charge redistribution times. The random gap breakdown isolates small pockets of charge in the transmitter, and therefore results in incomplete charge redistribution. Aside from minimizing these unwanted capacitances, the transmitter should be symmetrical to help suppress undesired modes. Section C below analyzes the interrelation between external and stray capacity, charge redistribution, and multiple-gap synchronization. It is assumed that systematic nonrandom gap breakdown occurs — the worst possible case.

C. Analysis of Charge Redistribution

A portion of a magnetic dipole transmitter, containing N identical capacitors C_i, is shown in Fig. 2. The capacitors are charged in parallel to identical voltages V, and subsequently discharged through N identical spark gaps. Let the external capacity between adjacent capacitor plates (and across each spark gap) be designated C_e. Assume the stray capacity from the transmitter to ground consists of 2N lumped capacitors C_s, located between each gap terminal and ground. Furthermore, assume all dissipative losses negligible. Before the first gap is discharged, the only fields existing around the transmitter are electrostatic and the line integral of the electric intensity around a closed path, such as the periphery of the transmitter, is zero.

4

Fig. 2. Portion of magnetic dipole transmitter.
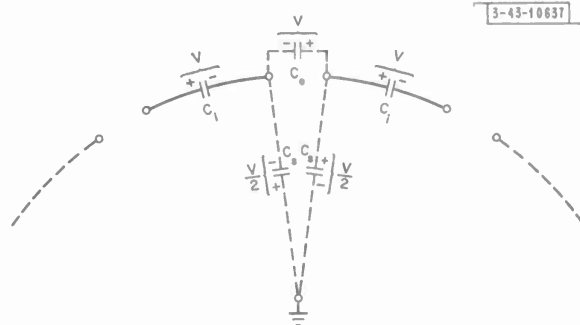
The potential difference between the outside of adjacent capacitors (or across the spark gaps) is, therefore, equal and opposite to the potential difference V across each capacitor. Furthermore, assuming the capacitors are charged from a balanced power supply, the potential across each lumped capacitor C_s will be $V/2$ as shown. The total internal energy initially stored by the transmitter is

$$N(\frac{1}{2} C_i V^2) \quad . \tag{8}$$

The total external energy initially stored is

$$N(\frac{1}{2} C_e V^2) + 2N [\frac{1}{2} C_s (\frac{V}{2})^2] \tag{9}$$

or

$$\frac{1}{2} NV^2 \left(C_e + \frac{C_s}{2}\right) \quad . \tag{10}$$

Assume that systematic nonrandom gap breakdown occurs (the worst possible case), resulting in complete symmetrical charge redistribution. Just before the last gap breaks down, and the transmitter radiates its stored energy, all the fields can again be assumed electrostatic. Because of the charge redistribution, the voltage across each capacitor is now V' and across the last gap is, therefore, NV'. Maximum voltages ($NV'/2$) of opposite polarities appear on the two stray capacitors located between the last gap and ground, and minimum voltages (0) appear on the diametrically opposite two capacitors. The voltage on intermediate capacitors ($2C_s$) varies in steps of V'. The final internal energy now stored by the ring is

$$N(\frac{1}{2} C_i V'^2) \quad . \tag{11}$$

The final external energy stored by the ring, and to be discharged imminently in the form of parasitic oscillations, is

$$\frac{1}{2} C_e (NV')^2 + 2 \{ \frac{1}{2} C_s (\frac{NV'}{2})^2 + \frac{1}{2} C_s (\frac{NV'}{2} - V')^2 + \ldots$$

$$+ \frac{1}{2} C_s [\frac{NV'}{2} - (N - 1) V']^2 \} \tag{12}$$

or

$$\frac{1}{2} C_e N^2 V'^2 + C_s V'^2 \sum_{n=0}^{N-1} (\frac{N}{2} - n)^2 \quad . \tag{13}$$

5

Equating the total initial energy stored in the transmitter to the total energy stored just before the last gap breaks down results in[†]

$$N\left(\frac{1}{2} C_i V^2\right) + \frac{1}{2} NV^2\left(C_e + \frac{C_s}{2}\right) = N\left(\frac{1}{2} C_i V'^2\right) + \frac{1}{2} C_e N^2 V'^2$$

$$+ C_s V'^2 \sum_{n=0}^{N-1} \left(\frac{N}{2} - n\right)^2 \tag{14}$$

$$V'^2 = \frac{V^2\left(C_i + C_e + \frac{C_s}{2}\right)}{C_i + NC_e + \frac{2C_s}{N} \sum\limits_{n=0}^{N-1} \left(\frac{N}{2} - n\right)^2} \tag{15}$$

For practical values of N under consideration (N = 10 to 100),

$$\frac{2}{N} \sum_{n=0}^{N-1} \left(\frac{N}{2} - n\right)^2 \approx \frac{N^2}{6} \tag{16}$$

therefore, with sufficient accuracy,

$$V' = V \sqrt{\frac{C_i + C_e + \frac{C_s}{2}}{C_i + NC_e + \frac{N^2 C_s}{6}}} \tag{17}$$

The transmitter operating efficiency η may be defined as

$$\eta = \frac{\text{desired energy output}}{\text{total energy input}} \times 100 \text{ percent} \tag{18}$$

or

$$\eta = \frac{N\left(\frac{1}{2} C_i V'^2\right)}{N\left(\frac{1}{2} C_i V^2\right) + \frac{1}{2} NV^2\left(C_e + \frac{C_s}{2}\right)} \times 100 \text{ percent} \tag{19}$$

By substituting the value of V' derived previously, Eq. (19) reduces to

$$\eta = \frac{C_i}{C_i + NC_e + \frac{N^2 C_s}{6}} \times 100 \text{ percent} \tag{20}$$

It is evident from Eq. (20) that even for small values of stray and external capacities the efficiency drops rapidly for any practical value of N. In the non-ideal case, however, two important factors operate toward increasing this theoretical "worst-case" efficiency. Gap breakdown will in all probability be of a random or semi-random nature, resulting in incomplete

---

[†]This is correct only where dissipative losses, such as the partial radiation resistances, as well as spark and circuit losses, are neglected. Due to the complexity of the ensuing analysis, this is the present assumption.

charge redistribution; the distributed inductances of the gaps and circuits will slow the charge-redistribution times, typically to the order of several to tens of nanoseconds. Gap synchronization should be accomplished faster than this. Nevertheless, the importance of minimizing stray and external capacities, as well as tolerances on the symmetry of the transmitter, should be recognized.

D. Fundamental Constraints

The theoretical maximum peak power that it is possible to radiate from such a transmitter has been calculated by Landecker,[1] and is reconsidered here with some modified assumptions but identical results. The peak power as given by Eq. (3) is transcribed below:

$$\hat{P} = \frac{2W\omega}{Q} \, e^{-\pi/2Q} \qquad [\text{Eq. (3)}]$$

Substituting values of W from Eq. (2), multiplying the numerator and denominator by Q, and using Eq. (1) result in

$$\hat{P} = \frac{N^2 V^2}{R_{RT} Q^2} \, e^{-\pi/2Q} \tag{21}$$

For possible values of D/λ under consideration, the first term of Eq. (5) may be used with sufficient accuracy to yield

$$\hat{P} \cong \frac{N^2 V^2 \lambda^4}{20\pi^6 Q^2 D^4} \, e^{-\pi/2Q} \tag{22}$$

Use of present-day dielectrics for the capacitors makes possible a dielectric strength of 1000 volts/mil (4×10^7 volts/meter), although this will vary with the thickness under consideration. Assuming that as much as one-quarter of the loop circumference ($\pi D/4$) is available for the dielectric (this is reasonable, as the present transmitter uses one-eighth), and the remainder for plates, gaps, and circuits, the total voltage NV impressed around the loop would be $\pi D \times 10^7$ volts. In order to get a pulse length of at least several cycles, Eq. (4) shows that Q must not be much smaller than 10. Substituting this minimum value of Q, as well as the maximum impressed loop voltage NV, into Eq. (22) gives

$$\hat{P} \cong \frac{5 \times 10^{10} \lambda^4}{\pi^4 D^2} \tag{23}$$

The minimum practical value of D/λ is between 0.2 and 0.3 (depending on the wavelength), even in the lossless case, since smaller values will result in excessively large mean-conductor diameters through the interrelation of Eqs. (5) and (7), and the assumed value of Q. Substituting the value of D/λ discussed above, and expressing the results in terms of the operating frequency f, yield

$$\hat{P}_{max} \cong \frac{10^{27}}{f^2} \tag{24}$$

The corresponding maximum energy radiated per pulse can be immediately ascertained from Eq. (3) as

7

$$W_{max} \cong \frac{10^{27}}{f^3} \quad . \tag{25}$$

Table I tabulates the limiting parameter values theoretically predicted by Eqs. (24) and (25) as a function of frequency, as well as the median resultant transmitter diameter. It is apparent that practical-sized transmitters are confined to the 1- to 1000-MHz range. There is no theoretical lower frequency limit, although a high-frequency limitation exists and is discussed below.

TABLE I MAXIMUM PREDICTED TRANSMITTER PARAMETERS				
Frequency (MHz)	1	10	100	1000
$\hat{P}_{max}$ (MW)	10^9	10^7	10^5	10^3
W_{max} (J)	10^9	10^6	10^3	1
Median diameter (ft)	300	30	3	0.3

The maximum theoretical operating frequency is determined by the minimum time of energy transfer t between adjacent capacitors. If the discharge path consists of n sections of equivalent lengths s_n (capacitor dielectric, gap supports, arc path, etc.), encompassed by respective relative permeabilities μ_{rn} and relative permittivities ϵ_{rn}, then the minimum energy transfer time will be

$$t = \sum_{n=1}^{n} \frac{s_n \sqrt{\mu_{rn} \epsilon_{rn}}}{c} \tag{26}$$

where c is the velocity of light. By allowing only 1/4 inch per section and leaving 1/16 inch for a high-dielectric material, a maximum theoretical operating frequency on the order of 10 MHz is predicted. This frequency cannot be attained practically since, aside from the size limitations implied in Table I, gap synchronization would have to be accomplished within a few picoseconds for successful transmitter operation. As will be shown in Sec. III, state-of-the-art synchronization times will probably limit transmitter operation to several hundred megahertz even under ideal conditions.

E. Signal Bandwidth Calculation

The wave emanating from the magnetic dipole transmitter takes the form of an exponentially decaying underdamped sinusoid. Considering only one section of the transmitter, the current i(t) flowing in the basic RLC circuit at any time is

$$i(t) = I_o e^{-t/2\tau} \sin \omega_o t \tag{27}$$

and the voltage across the resistance e(t) is just

$$e(t) = i(t)R \tag{28}$$

where

8

$$I_o \equiv \frac{V}{\omega_o L} \tag{29}$$

$$\tau \equiv \frac{L}{R} \tag{30}$$

$$\omega_o = \sqrt{\frac{1}{LC} - \left(\frac{R}{2L}\right)^2} \quad \text{for } R < 2\sqrt{L/C} \tag{31}$$

The energy radiated from the circuit per section, considering the lossless case ($R = R_R$), is given by

$$\frac{W}{N} = \int_{-\infty}^{\infty} i(t)\, e(t)\, dt \tag{32}$$

which can be equated by use of the Fourier transform and Parseval's formula[10] to

$$\frac{W}{N} = \frac{1}{\pi} \int_{O}^{\infty} F_1^*(\omega)\, F_2(\omega)\, d\omega \tag{33}$$

where $F_1(\omega)$ corresponds to i(t), and $F_2(\omega)$ corresponds to e(t). Performing the required operations results in

$$\frac{W}{N} = \frac{LI_o^2}{2} \cdot \frac{1}{1 + \frac{1}{4Q^2}} \tag{34}$$

which, of course, converts directly into the known relation

$$\frac{W}{N} = \frac{CV^2}{2} . \tag{35}$$

The product of $F_1^*(\omega)\, F_2(\omega)$, however, represents the energy spectrum of the waveform and is

$$F_1^*(\omega)\, F_2(\omega) = \frac{I_o^2 \omega_o^2 R}{\omega^4 + \omega^2 \omega_o^2 \left(\frac{1}{2Q^2} - 2\right) + \omega_o^4 \left(1 + \frac{1}{4Q^2}\right)^2} \tag{36}$$

Normalized, Eq. (36) can be rewritten for $Q > 1$ as

$$[F_1^*(\omega)\, F_2(\omega)]_N = \frac{\omega_o^4/Q^2}{\omega^4 + \omega^2 \omega_o^2 \left(\frac{1}{2Q^2} - 2\right) + \omega_o^4 \left(\frac{1}{2Q^2} + 1\right)} \tag{37}$$

and is plotted in Fig. 3 for values of Q = 10, 20, and 100. Graphical integration of Fig. 3 shows that the respective bandwidths containing 90 percent of the total energy are ± 20, ± 10 and ± 2 percent. These bandwidths compare to an equivalent rectangular RF pulse of length T such that

$$T = 3\tau . \tag{38}$$

F.   Signal Modification

A short computer analysis was undertaken in order to explore the possibility of modifying the exponentially decaying waveform of the transmitter to the more accepted rectangular format. One expedient and proven method is to couple parasitic elements to the transmitter. However,
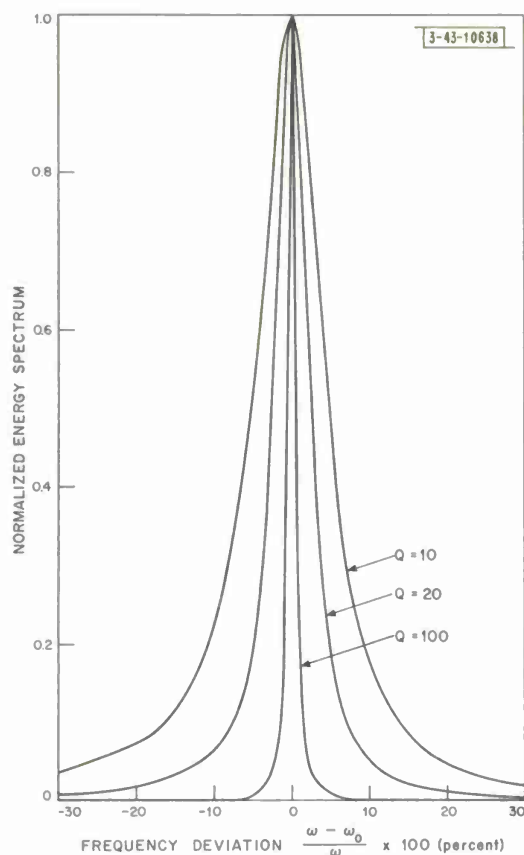
9

Fig. 3.   Energy spectrum of transmitted waveform.

this results basically in changing the effective Q, and therefore only the decay rate, of the waveform.   In order to modify its form, the possibility of replacing the energy storage capacitors with "RF pulse-forming networks" (i.e., combinations of LC circuits) was investigated. Aside from appearing difficult to implement on a practical transmitter, the results seem to indicate nonattainment of the desired rectangular format.   The analysis was not completed since excessive computer time was involved, but it appears that the resulting waveform consists of a combination of exponentially decaying signals of different frequencies.   Undoubtedly, these frequencies combine to produce a waveform resembling a negatively matched multisection pulse-forming network.

III.   INVESTIGATION OF GAP CHARACTERISTICS

The only active elements in the transmitter, and consequently those requiring detailed examination, are the energy transferring switches whose desired characteristics are: very small size, high-voltage holdoff, near-instantaneous and controlled switching performance, and extremely high current-conducting capability with small associated losses.   The one device that even remotely approaches these characteristics, which are quantitatively described in Sec. IV, is the spark gap.   Accordingly, a theoretical and experimental investigation was undertaken to study those aspects of gap operation which relate directly to total transmitter performance.

A.   Essential Spark-Gap Theory

The basic factors of accepted spark-gap theory are reviewed below in order to prepare for an understanding of work described in succeeding sections.   The principles discussed are

10

necessarily brief and incomplete, and opposing explanations sometimes exist which are not developed.   A complete treatise may be found in the literature referenced in the succeeding paragraphs.

A spark gap in the OFF state, as defined here, consists of a pair of charged electrodes separated by a gas in which an electric gradient exists by virtue of the electrode potentials.   In the ON state, gap breakdown has been accomplished and a self-sustained discharge having a high current density with a low voltage drop (i.e., low arc impedance) exists across the gap.   The transformation phenomena between the OFF and ON states of the gap, as well as the ON impedance of the gap, are the principal areas of immediate concern.   These phenomena can be conveniently grouped into three time-dominated categories: the statistical, the formative, and the transition stages.   The latter category in itself encompasses an initial and a final stage.

When a voltage in excess of the static breakdown voltage is applied to a gap, there is a time delay, statistical in nature, before any discharge buildup occurs.[11] This statistical delay is the time required for an electron to appear in the gap and subsequently initiate the breakdown process.   Without this discharge-initiating-electron, gap breakdown will not occur no matter how much the applied voltage is increased.   Practically, however, at these high overvoltages this discharge-initiating electron will be supplied by locally enhanced field emission or directly from the negative ions present in the gas.[12] Natural sources of discharge-initiating electrons include those generated by cosmic radiation and natural radioactivity in surrounding materials, as well as attendant thermionic emission and interpulse surviving electrons in repetitive applications. Artificial background radiation, such as provided by radioactive materials, x-ray generators, and ultraviolet and laser sources, is a more reliable means of producing the necessary discharge-initiating electron.   Ultraviolet and laser radiation of sufficient intensity, as well as being more effective and easier to implement than other methods,[13] can lower the threshold field required for breakdown.   This effect will be discussed in Secs. III-B and -C.   From the above paragraph, it is evident that the statistical time delay can be reduced to zero by providing a constant source of free electrons.

The formative lag of the spark gap is generally accepted to be the time for an initial electron avalanche to build up a space-charge field comparable with the externally applied field.[14] At this point, the preliminary spark channel is established, in a time negligible compared with the initial avalanche formation, by streamer propagation (secondary avalanches diverted to the main avalanche) precipitated by photon emission from the highly ionized gas.   Calculations of the formative lag imply that for any given gas the time delay should be a function of the applied field and gas pressure only: Actually, it has been found experimentally[15] that for low fields (small overvoltages) the time delay also depends on the gap width or applied voltage.   It is believed that, for the low fields, multiple avalanches are required to create the necessary space charge. However, it can be stated with sufficient accuracy that for any set of gas and electrode parameters the formative lag time for an overvoltaged gap will vary inversely with the percentage of gap overvoltage and gas pressure.   The theoretical and experimental formative lag times for different gas and electrode parameters have been investigated by several workers and are well documented in the literature.[16-18] Figure 4 is a composite plot of these data and is approximately valid for most practical air and nitrogen gaps.   Conflicting theories of the formative breakdown process exist,[19] but all predict the same order of formative lag times discussed.

The preliminary spark channel that has been established by the formative process is a relatively low ion-density streamer and will not sustain an external current.   The processes
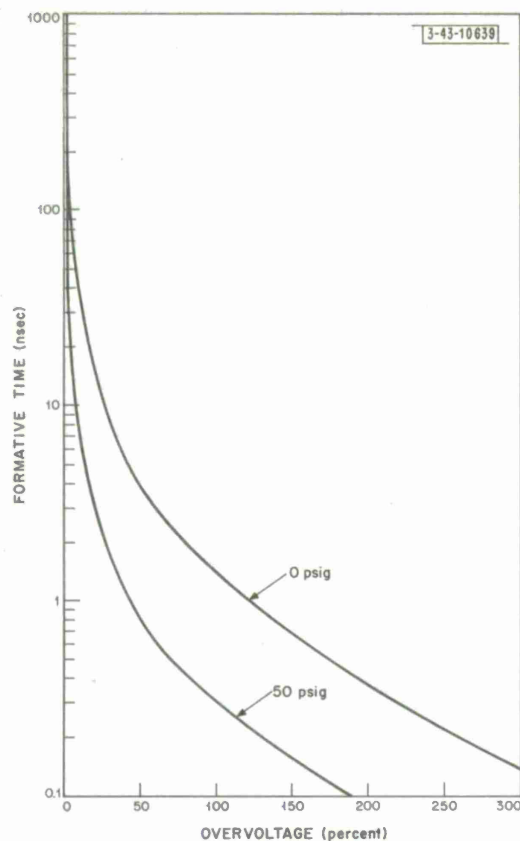
11

Fig. 4. Consolidated formative time data for air and nitrogen gaps.

involved in the transition of this streamer to the final low-impedance spark channel are not well understood, and little theoretical or experimental work exists. It appears that the same factors which determine the formative lag time affect the transition time which, by observation,[20] is somewhat faster. Experiments have also been performed[21] which indicate, in addition to the factors outlined above, a linear relationship between gap spacing and transition time. It is likely that there is an initial transition time in which the external current rises to a large fraction of its ultimate value, while the arc channel expands rapidly at a rate on the order of the thermal velocity of the gas atoms. The final transition time, which is longer, involves diffusion of gas particles and sheath formation.

The form of the DC or low-frequency gap impedance in the ON state is well documented and consists of a negative-resistance region which transforms to a constant arc drop at higher current levels. At high frequencies (above 1 kHz to 1 MHz, depending on gas and electrode parameters), the volt-ampere characteristic has become essentially that of a pure resistance[22] because the gas ionization level cannot conform to the rapid alternations in current. Theoretical and experimental work is sketchy, and the only available data[3,23,24] suggest a dynamic arc resistance of several ohms per centimeter, varying linearly with arc length, in the 20- to 40-MHz range at gas pressures of 0 and 50 psig. The corresponding inductance appears to be several nanohenries for a 1-cm gap — the inductance not varying linearly with length. Since the diameter of an arc channel is a slowly varying inverse function of the gas pressure, this inductance should increase slightly with pressure. No other appropriate data are known to exist.

The type of fill gas used has some relationship to all the parameters mentioned. This dependence will be examined in Sec. III-C. Obviously, pure dry air is easily available and has been

12

used by many workers with good success. Another commonly used gas, nitrogen, is not too satisfactory because self re-ignition of the arc takes place readily. Nitrogen ions, as well as other simple and monatomic ions, cannot dissociate and, when being neutralized by an electron, will emit photons to start the breakdown process again.[25] The addition of attaching gases, which capture electrons, or a polyatomic quenching or dissociating agent to such a gas will help absorb this photon energy and allow proper extinction of the arc. A successful mixture, used by some researchers,[26] consists of $90\% N_2 - 10\% CO_2$ by volume. This mixture results in fast stable breakdown and controlled extinction, whereas in pure nitrogen spontaneous breakdown and re-ignition occur, and in pure carbon dioxide nonpredictable and slow breakdown ensues.

B. Gap-Triggering Processes

In order to initiate the gap breakdown, sufficient ionizations of the fill gas must be accomplished by some triggering process as outlined in Sec. A above. This may be achieved by increasing the field-to-pressure ratio directly or by injecting into the gap ions or electrons which effectively enhance the local field. Increasing the field-to-pressure ratio by changing either the gap spacing or pressure is obviously a relatively slow process. On the other hand, overvolting the gap is generally recognized as the fastest means of initiating breakdown. The voltage pulse may be applied directly across the gap or to some auxiliary electrode,[27,28] thereby distorting a portion of the electric field. If statistical times are negated and transition times are a function of formative times, as implied in Sec. III-A, then Fig. 4 is indicative of total gap-breakdown times (the overvoltaged portion) if the ordinate is multiplied by some factor between 1.0 and 2.0.

An indirect method of overvolting a gap near threshold is to illuminate the gap with laser, ultraviolet, or x-radiation. The radiation causes direct ionization of the gas and/or photo emission at the cathode producing sufficient electrons, by the mechanism of inverse bremsstrahlung, to distort the field and initiate breakdown. Photo emission at the cathode, the most accepted mechanism, is obtained when a photon of laser, ultraviolet, or x-radiation impinging on it has an energy hf larger than the energy $e\varphi$ required to transfer an electron through the photoelectric work function φ. The emitted electron can have a maximum energy, $1/2\,mv^2$, such that

$$\frac{1}{2}\,mv^2 = hf - e\varphi \quad . \tag{39}$$

As the space-charge cloud forms and drifts toward the anode, the local field is distorted and initiates the breakdown process. Since more than one mechanism is involved, total gap-breakdown times would be longer than for externally overvoltaged gaps. Direct ionization of the gas by multiple-step ionization, however, is a possibility that cannot be precluded. This process would yield faster breakdown times. To achieve direct ionization, the photons must either have an energy hf larger than the ionization energy eVi of the gas atoms, or accumulate an energy Σhf inside the respective atoms.[29] In this instance, as the stacked photon energy exceeds that required for ionization, the probability of ionization diminished rapidly. The number of electrons emitted per second is, in either case, proportional to the intensity of the incident radiation. Furthermore, the electron emission lags the photon arrival by subnanosecond times, and thus produces negligible statistical time delays without the use of artificial background radiation.

Effective ultraviolet radiation is limited to wavelengths encompassing 3000 to 1000 Å. Nitrogen absorbs wavelengths shorter than 1000 Å quite readily, carbon dioxide absorbs those shorter than 1600 Å, and oxygen has a complex absorption profile containing several windows in the

13

region of interest.[30] Photons of wavelengths longer than 3000Å generally do not possess sufficient energy to accomplish ionization. A convenient and efficient source of high-intensity ultraviolet radiation encompassing the proper spectrum is an auxiliary spark discharge. Other sources of ultraviolet, such as gas discharges or the barium-titanate tungsten-whisker device, do not produce sufficiently intense radiation. In order to optimize the production of the desired radiation, researchers have experimented with several gap materials and geometries.[31] Silver-loaded graphite gaps proved somewhat superior to copper-loaded graphite, pure graphite, and brass in ultraviolet production, but none were particularly erosion-proof. Longer gap spacing, obtained through a reduction in pressure or by the use of sharper electrodes, increased both the ultraviolet source size and intensity. The reliability of ionization is affected by the source size and intensity, the distance between the ultraviolet source and the main gap, the angle of the incident radiation, the voltage of the main gap relative to self-breakdown, and, to a lesser extent, by the absolute voltage of the main gap.[32] High peak ultraviolet intensity, especially during the first few nanoseconds, is more significant in effecting ionization than total integrated energy. Short ultraviolet rise time will, of course, result in minimum jitter. The overall efficiency of photoelectric conversion can be calculated from available data[32] and varies between 0.004 and 4 percent, depending on the assumed photon energies and cathode surfaces. For example, 25 to 25,000 electrons passing through a spark generate a sufficient number of photons so that if all impinged on the main-gap cathode, the probability is that one photoelectron would be emitted. Data taken by researchers in the field[31] for a 30-nsec, 4-J ultraviolet trigger derived from an auxiliary spark 6 inches from the main gap are reproduced in Table II. Note that for minimum jitter and delay, the main gap must be very close to self-breakdown. Furthermore, multiple gaps charged from a common supply and not possessing the same self-breakdown voltage will have unequal delay times. These phenomena, in addition to the jitter, will inhibit proper gap synchronization.

An improvement in the reliability, jitter, and operating range of ultraviolet triggering can be obtained by applying an overvoltage to an auxiliary triggering electrode on the main gap

| TABLE II | | |
ULTRAVIOLET TRIGGERING DATA		
Self-Breakdown (percent)	Average Delay (nsec)	Jitter (nsec)
98.3	77	1.6
96.7	82	1.8
95.0	88	2.1
93.3	95	2.8
91.7	106	3.0

Conditions:

4-J, 30-nsec trigger from silver-loaded-graphite auxiliary gap

6-inch spacing

Nitrogen atmosphere

14

immediately after the ultraviolet illumination. The success of this method depends on the high levels of pre-ionization present in the gas, as a result of the ultraviolet radiation, when the overvoltage is applied. A delay in the application of overvoltage of some 15 nsec has been found optimum in reducing jitter.[33] This time is probably required to establish proper levels of pre-ionization.

Illuminating a gap by means of a flash x-ray source results in performance similar to ultraviolet triggering. A recent experiment using a 150-kV source providing a 50-nsec dose of 35 mR at the main gap resulted in reliable triggering down to 90 percent of the self-fire limit. No time-delay measurements were taken. The complexity of this triggering method, however, probably inhibits its usefulness.

Laser-induced gap breakdown, in addition to offering the optical beam-splitting and electrical isolation characteristics of ultraviolet triggering, can produce localized alternating electric fields 300 times greater than the self-breakdown fields of typical atmospheric gaps. Therefore, no polarization effects are evident. Although the breakdown mechanism is believed to be similar to the general ultraviolet model previously described, a detailed theoretical description is not presently available. Recent experiments[34] performed with a Q-spoiled chromium-ruby laser produced results at least comparable to those obtainable with ultraviolet triggering. The 0.8-J, 10-nsec laser output created alternating fields of approximately 10^6 volts/cm at the focal point of a 50-mm lens. These fields, when focused between the electrodes, successfully triggered atmospheric gaps near threshold with approximately 50-nsec delay and 10-nsec jitter. With the focal point at the cathode-electrode delay times dropped below 10 nsec, jitter was not measured. Furthermore, these results were not affected by a reduction in laser power down to some critical value — about 6 MW for the experimental arrangement described. Reliable triggering, although accompanied by excessive delay times, was obtained down to 30 percent of the gap self-breakdown field strength. Further research is being performed in this area, and the expected results could make laser triggering a most inviting solution to many existing problems.

The use of coherent RF energy to initiate gap breakdown, although attempted in the field,[3] does not work because the photon energy involved is many orders of magnitude too small. Extremely high RF fields, if they can be produced, would tend to initiate gap breakdown at levels approaching the breakdown of the atmosphere.

Finally, the triggering of a gap through the direct injection of ions or electrons is not practical. A scheme which accomplishes this concurrently with other mechanisms, but is usually deferred in favor of the trigger-electrode gap, is the placement of an auxiliary gap inside the main gap. This auxiliary spark not only produces ions or electrons which precipitate local variations in the field, but creates ultraviolet radiation and a low-pressure region caused by the dissipated trigger energy. All these factors tend to support imminent breakdown.

C. Experimental Investigations

The lack of undisputed theory and detailed data on gap operating parameters, evident in the previous sections, necessitated an experimental determination of these factors. Accordingly, a pressure vessel consisting of a cylindrical shell with hemispherical heads was constructed. The vessel, which is 24 inches in diameter and 40 inches long, has an allowable working pressure of 175 psig. Figure 5 is a photograph of the unit. The inclusion of a 12-inch-diameter
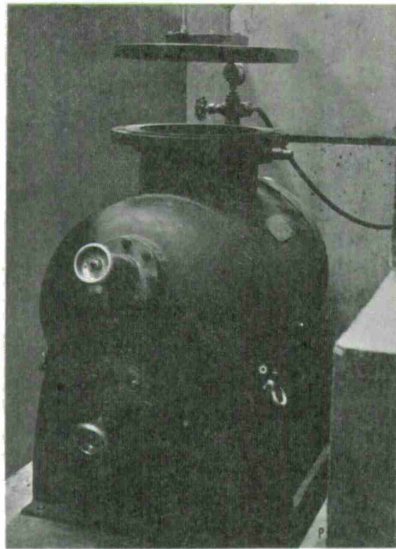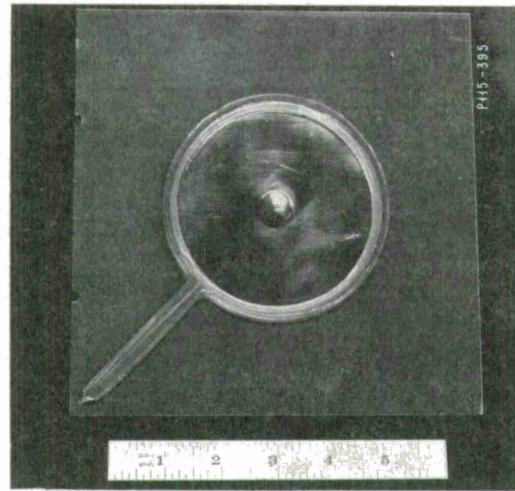
15

Fig. 5.   Pressure vessel.

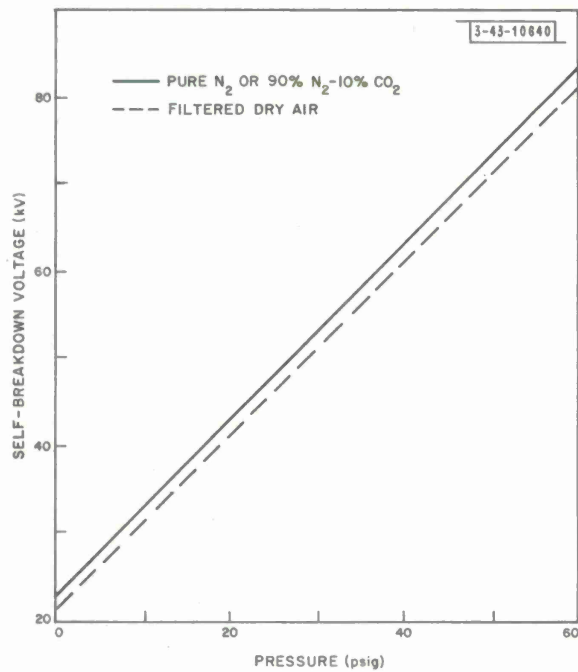Fig. 6.   Representative transmitter section.

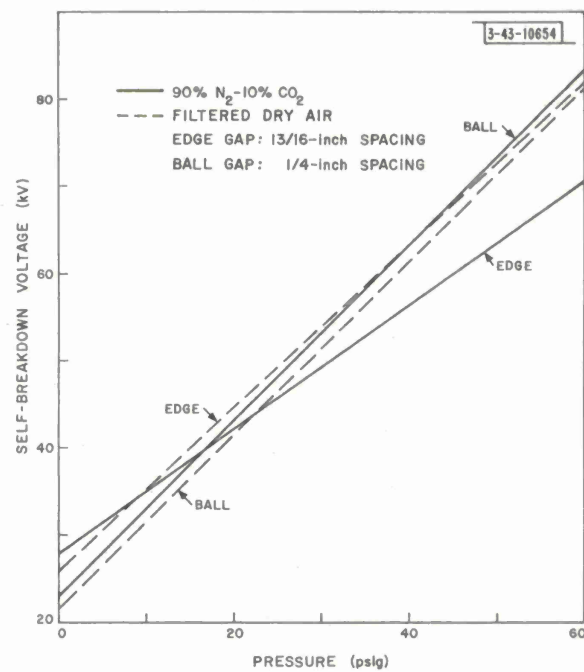Fig. 7.   Self-breakdown voltage of transmitter gaps.

Fig. 8.   Breakdown voltage of thin edge vs ball gap.

access opening, a 4-inch-diameter sighting glass, four high-voltage feedthrough connectors capable of 100-kV tandem operation, two high-voltage RF connectors, several low-voltage terminals, as well as pressure inlet and outlet valves, makes this a very versatile test chamber.

In order to limit the extent of the investigation, all data were taken with a single representative spark gap taken from the final transmitter design. Essentially, this gap consisted of 5/8-inch-diameter aluminum half-spheres separated by 1/4 inch and centered on 3-7/8 inch-diameter copper-clad laminated plates. The plates actually form one-half of the energy storage capacitors described further in Sec. IV-B. Figure 6 is a photograph of a representative transmitter section showing one of the gaps and plates. Since many of these sections are arranged in a circular format in the final transmitter design, the outer side of the copper plates is separated by approximately 15/16 inch, whereas the inner spacing is only 13/16 inch.

Data of the self-breakdown voltage as a function of gas type and pressure, correlated with accepted breakdown theory and the results, are plotted in Fig. 7 for reference. Pressurization not only allows higher charging voltages, but also modifies spark-gap performance favorably. No appreciable difference in results was noted whether pure nitrogen or the $90\% \, N_2$-$10\% \, CO_2$ (90-10) mixture was used, or if the applied voltage was balanced or referenced to ground. As expected, the arc channel extinguished properly both in air and in the 90-10 mixture. In a pure nitrogen atmosphere, however, extinction was prolonged and erratic. Further use of pure nitrogen was discontinued since it offers no particular advantages over the 90-10 mixture. The mixture, as well as pure nitrogen, produced anomalous arc and glow discharges at higher pressures. Normal behavior was observed in the unpressurized region, whereas with slight pressurization the arc tended to transfer from one of the gaps to the edge of the negative copper plate. At higher pressures, the discharge occurred completely between the inner edges of the copper plates with attendant glow and sputtering from the positive plate. This effect was also observed to a lesser degree at much higher pressures (over 60 psig) in an air atmosphere. It was presumed that a different slope and attendant crossover occurs in the thin edge vs the ball-gap breakdown curves at the higher pressures. Subsequent data, obtained and reproduced in Fig. 8, indicate that this phenomenon is indeed present. In order to suppress these anomalous discharges, modification of the relatively thin edge of the copper was attempted. Dip soldering, electroplating, and small-diameter corona rings all proved unsuccessful, as the edge could not be modified sufficiently. Coating the plates with dielectric materials, including teflon pressure-sensitive tape, CTF teflon spray, corona dope, and several polyurethane resins, was also unproductive because of the presence of trapped air and/or excessive pinholes. A 3/32-inch coating of RTV-108 (a silicone rubber manufactured by the General Electric Company) applied along the edges of the copper finally provided the required modification. This solution not only reduced trapped air and pinholes to a minimum, but reduced the electric-field gradient near the plates by virtue of the larger effective dielectric diameter and its larger dielectric constant.

The first series of gap experiments was concerned with measuring the transition time and the high-frequency impedance of a representative transmitter spark gap as a function of gas type and pressure. As mentioned previously, theoretical and experimental information is almost nonexistent in these areas. The experimental arrangement represented in Fig. 9 was used to obtain the transition time data which also yielded transient DC gap-impedance information. The test setup, a coaxial low-inductance arrangement, is capable of response times under 1 nsec. The pulse balun, sometimes used to reduce ground loops and delay the signal during
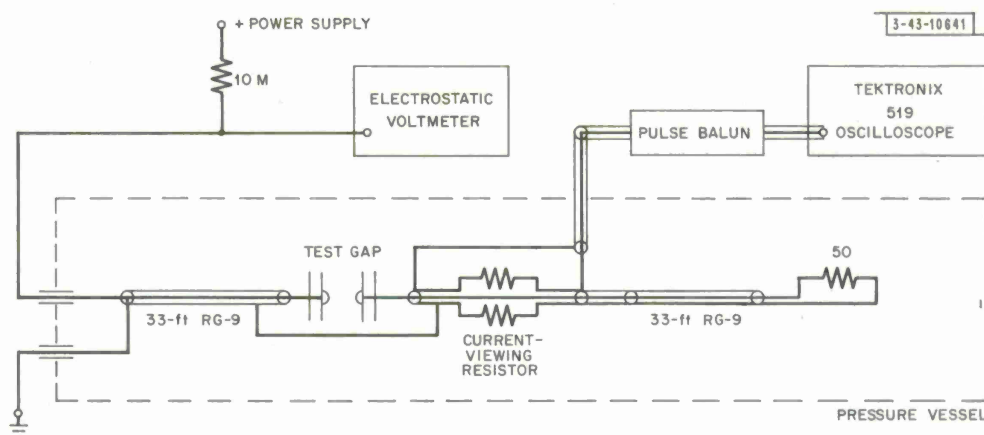
17

Fig. 9.   Test setup for temporal measurements.

period of high-RF interference, degraded response times to the order of 1 nsec.   A 70-kV coax-ial current-viewing resistor, custom designed by T&M Research Products, was used for instru-mentation.   Holes were drilled through the rear of the test gap to permit convenient connection of the charging cable to the input side of the gap and the current measuring equipment to the out-put.   A low-inductance plate was used to connect the ground shields of the cables.   Tests were performed by applying a slow DC overvoltage to the gap, in both an air and a 90-10 atmosphere, by means of the energy stored in the input coaxial cable.   Figure 10 shows typical gap-current responses obtained.   No difference in response was noted for positive- or negative-charging voltages.   The graph reproduced in Fig. 11 presents the results of the measurements.   The re-quirement for pressurization, and the advantages of a gas mixture such as the $90\% N_2 - 10\% CO_2$ used, are immediately evident for successful transmitter operation.

The high-frequency impedance of the transmitter gaps, for the slow DC overvoltage case, was measured using the experimental arrangement shown in Fig. 12.   Two representative trans-mitter units were connected by a copper strap whose inductance resonated with the unit capaci-tors such that, when shock-excited, the resultant oscillations of about 100 MHz were near the frequency of interest.   A small probe, placed several inches from the test gap, was used to couple a portion of the signal to the oscilloscope.   A representative picture of the resultant re-sponse is shown in Fig. 13.   The effective impedance was calculated by utilization of the loga-rithmic decrement.   The conclusions drawn from the data obtained indicated an RF impedance of approximately 0.95 ohm, not being an appreciable function of either gas type, gas pressure, or time after the transition stage.   These results agree in magnitude with the limited available data discussed in Sec. III-A.   The transient DC gap-impedance information, available as a by-product of the transition time experiment, indicates a gap impedance of several ohms which is also not a function of gas type and pressure.
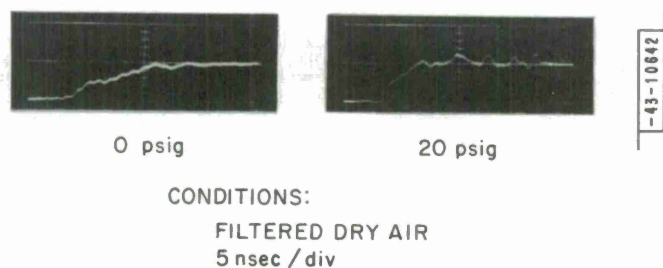

0 psig   20 psig

CONDITIONS:
   FILTERED DRY AIR
   5 nsec / div

Fig. 10.   Typical gap response for slow DC overvoltage.

18

Fig. 11.   Transition time for slow DC overvoltage.
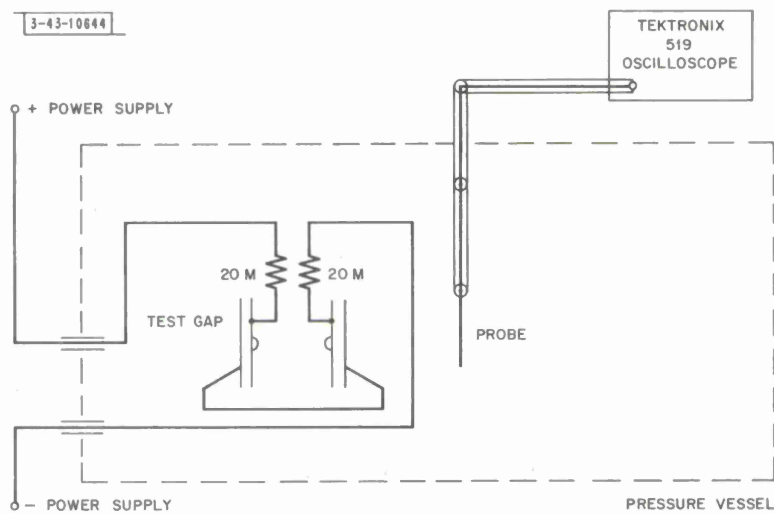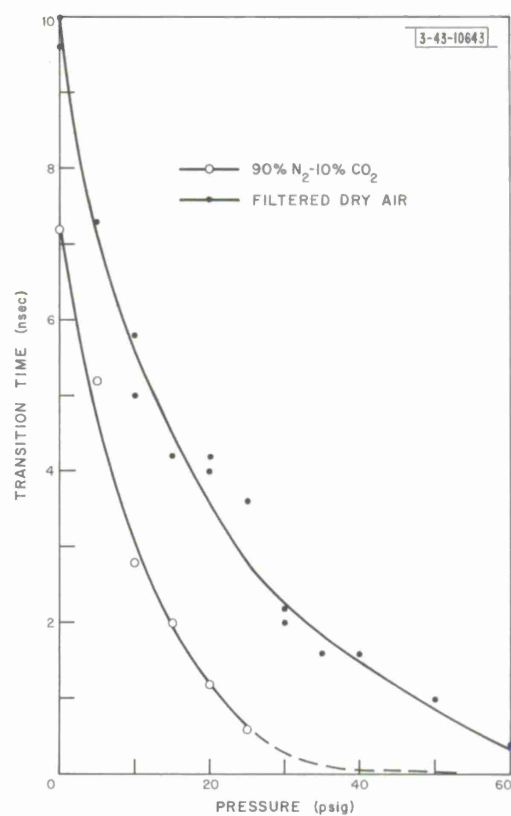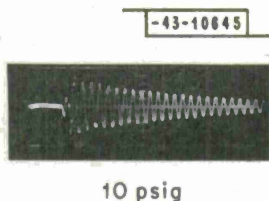

Fig. 12.   Test setup for impedance measurements.

-43-10645

10 psig

CONDITIONS:
FILTERED DRY AIR
50 nsec / div

Fig. 13. Shock-excited
gap response for slow
DC overvoltage.

Temporal measurements on a representative ultraviolet-triggered gap were obtained using the test setup (shown previously in Fig. 9) with the addition of an ultraviolet source and associate instrumentation. The ultraviolet radiation, produced by a 200-nsec, 5-J spark, emanated from the same source used in the full-scale transmitter described in Sec. IV-C. Oscilloscope triggers with calibrated delays, obtained from an auxiliary current-viewing resistor in the ultraviolet cable, allowed measurement of the formative and transition times of the representative gap as a function of gas type and pressure, ultraviolet intensity, and percentage of self-breakdown voltage. The first set of measurements, taken with an ultraviolet-to-main-gap spacing of 12 inches, represents the equivalent conditions, including the effect of the conical reflector, found in the full-scale transmitter. The results were discouraging and indicated a lack of sufficient peak ultraviolet intensity for proper triggering. Formative times were not an appreciable function of pressure and averaged 130 nsec in air and 100 nsec in a 90-10 atmosphere. Jitter was extreme approaching 45 and 20 nsec, respectively. Transition times for both atmospheres were similar to those shown in Fig. 11 for the slow DC overvoltage case, indicating a similar breakdown mechanism and, therefore, insufficient available triggering energy. Although the 90-10 mixture was definitely more stable and reliable, the overall response was still inadequate. Figures 14(a) and (b) are plots of the formative, jitter, and transition times as a function of the
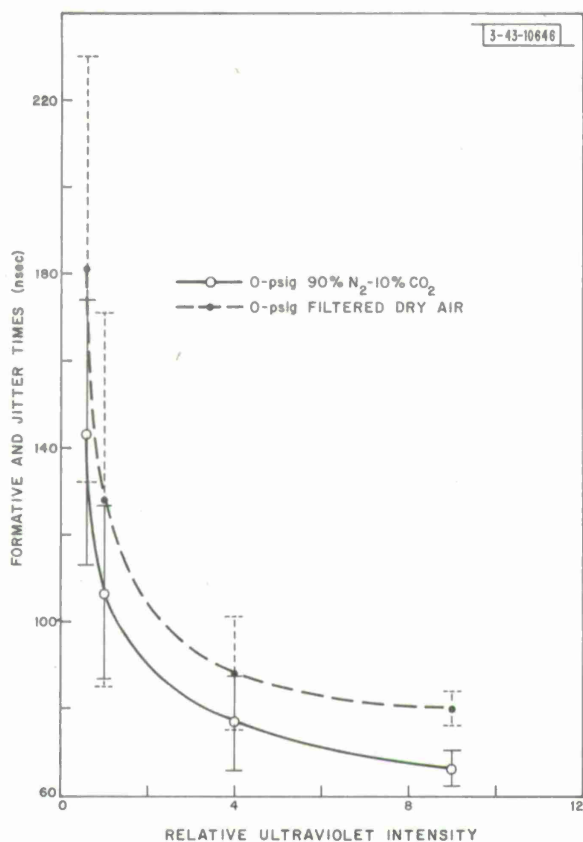

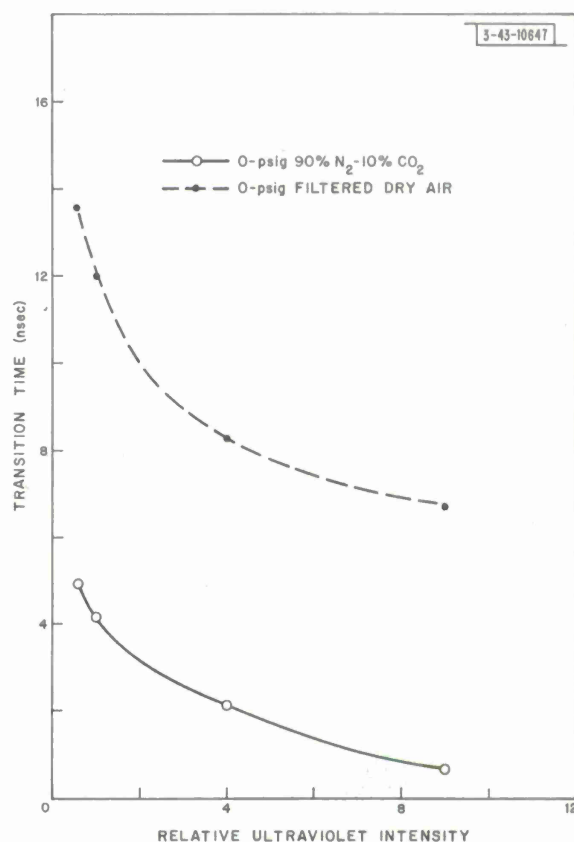Fig. 14(a). Formative and jitter times as a function of ultraviolet intensity.

Fig. 14(b). Transition time as a function of ultraviolet intensity.

available ultraviolet intensity for 0-psig gaps. The intensity was varied by changing the ultraviolet source to main-gap distance, a relative intensity of 1.0 representing the conditions existing in the full-scale transmitter. It is evident from these data that the peak intensity of the ultraviolet source used is 5 to 10 orders of magnitude low. This problem is discussed further in Sec. IV-C. The importance of adjusting and maintaining all gaps close to their self-breakdown voltage is restated through Fig. 15 which plots this parameter vs formative time. Successful triggering, using a relative ultraviolet intensity of about 10, was achieved to 93 percent of the self-breakdown voltage. Obviously, multiple-connected gaps cannot be charged any closer to their self-breakdown voltage than their adjustment tolerance. Thus, operation is forced further from the self-breakdown voltage of some gaps than desirable. Finally, gap impedance did not appear to be a function of any ultraviolet parameter described.

Fig. 15. Temporal measurements as a function of percentage of self-breakdown.
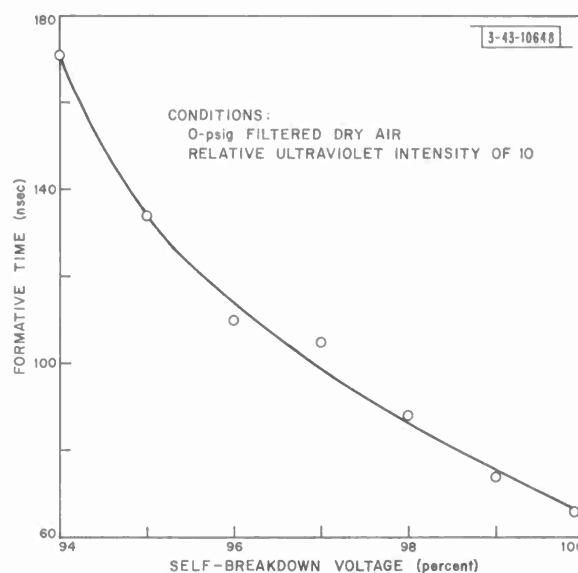
Experimental investigations of other gap-triggering processes were not performed because either the methods had no immediate practical transmitter application (alteration of pressure or spacing, flash x-radiation, direct gap injection), current research is being conducted in the field (laser-induced breakdown), or enough practical information for usable transmitter designs is presently available (pulsed overvoltage triggering).

IV. EXPERIMENTAL TRANSMITTER

The experimental vehicle used in this investigation of spark transmitters is the ring-form or magnetic dipole, as described previously. By applying the methods and equations outlined in Sec. II-A, the design tabulated in Table III was developed, fabricated, and experimentally evaluated. Two sets of parameter values are given: one for zero losses, the other for the total losses equal to the radiation resistance (a reasonable assumption). All calculations presumed 50-psig transmitter pressurization.

In order to calculate the inductance per section, which includes mutual effects, it was necessary to assume a reasonable value for the diameter of the mean current path. This was accomplished by allotting distinctive diameters to individual components and combining these in a length-weighted manner, resulting in a 0.388-inch-diameter current path. Furthermore, as

21

TABLE III		
EXPERIMENTAL TRANSMITTER DESIGN		
Parameter	Losses = 0	Losses = Radiation Resistance
Frequency (MHz)	135	135
Peak instantaneous RF output power (MW)	1260	1130
Total energy per pulse (J)	12.4	6.2
Pulse width to 10-percent power (nsec)	41	20.5
Signal bandwidth for 90-percent energy (MHz)	35	70
Total charging voltage (kV)	72	72
Mean radiating diameter (inches)	23.6	23.6
Diameter to wavelength ratio	0.27	0.27
Radiation resistance (ohms)	88.6	88.6
Total number of transmitter sections	74	74
Inductance per section (nH)	21.4	21.4
Capacitance per section (pF)	64.9	64.9
Operating quality Q	15.1	7.6

discussed previously, since the inductance of a spark increases slightly with pressure (due to a decreased spark diameter), the effect of transmitter pressurization on operating frequency was calculated. No frequency change, to four significant figures, was predicted as a result of increasing the pressurization from 0 to 50 psig.

The external capacity C_e between transmitter sections was calculated, and subsequently verified by measurement, to be 3 pF. Similarly, the stray capacity C_s between a half-section and ground was determined to be 1 pF, including the charging resistor capacity. Substituting these values into Eq. (20) would predict a worst-case transmitter efficiency of 5.4 percent for the charge-redistribution limited case. As discussed in Sec. II-C, this possibility (induced by complete charge redistribution) is not likely to occur.

A.   Physical Layout

The transmitter components are housed in a Rexolite framework which is enclosed by a low-loss pressurized radome. The framework consists of a hollow cylinder, 9-1/8 inches long, with an overall nominal diameter of 31 inches. Central access holes of 16-1/4 inches nominal diameter are located in each disk-shaped end. The walls of 1/8-inch-thick Rexolite 2200, after forming in a large oven, were cemented to the 1-inch-thick Rexolite 1422 disks with Rexolite 12517 adhesive. These materials were chosen for their low-loss relatively stable characteristics. Seventy-four equally spaced 1/8-inch-square radial slots were machined into the inner surfaces of the disks to accommodate the individual transmitter units which slide into the structure. Figure 16 is a photograph of the partially assembled structure. When fully assembled,
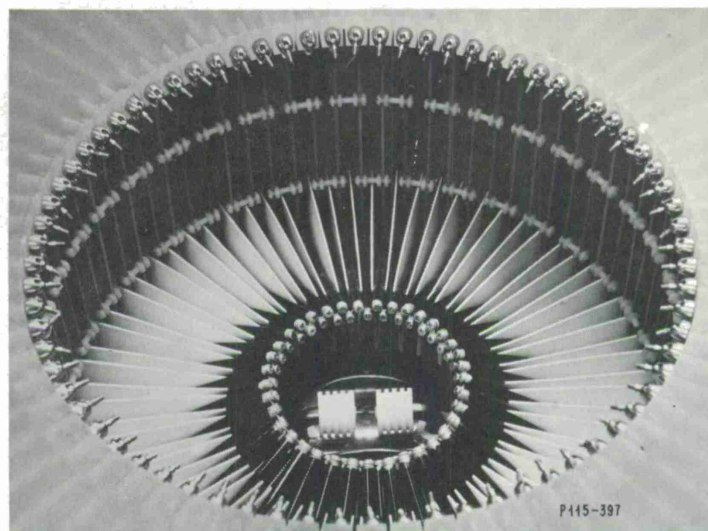
Fig. 16.   Partially assembled transmitter.

the upper half of the transmitter is identical to the lower half shown, except that the central
ultraviolet source is supplanted by a conical ultraviolet reflector.   The charging resistors are
conveniently connected to one side of the individual transmitter units by standard ballpoint-pen
swivel joints.   Teflon spacers, as shown, prevent flashover in the charging section of the trans-
mitter.   The circumferentially located nylon screws and nuts help maintain the desired gap
spacing of the transmitter units.

As outlined in Sec. II, transmitter symmetry and component tolerances are of prime impor-
tance in assuring successful transmitter operation, particularly under multiple-gap synchroni-
zation conditions.   Table IV indicates the tolerance allowed on the critical portions of the trans-
mitter.   All the tolerances were met except the specification on warp and twist of the laminated

| TABLE IV | |
TRANSMITTER TOLERANCES	
Transmitter Structure	
All critical dimensions and surfaces	± 0.001 inch
Laminated Plates	
Thickness	± 0.004 inch
Warp and twist	± 0.0035 inch
End milling	± 0.001 inch
Relative dielectric constant	± 0.05
Etching of copper	± 0.0025 inch
Relative positioning of copper	± 0.001 inch
Gap Structure	
Diameter of balls	± 0.0002 inch
Machining of balls	± 0.001 inch
Bonding of balls	± 0.0005 inch for jig

plates. This necessitated the addition of the nylon screws and nuts, as explained further in the following section.

B. Component Selection

Because of the combined requirements of symmetry, close and stable tolerances, restricted size, and high-voltage operation, components were selected, designed, and tested in detail. A description of this process, with the exception of the ultraviolet components which are treated separately in Sec. IV-C, follows.

1. Laminated Plates

The laminated plates are the core of the individual transmitter sections since they encompass the capacitors, serve as a base for mounting the gap structures, and form part of the sectional inductances. A photograph of such a transmitter section was shown previously (Fig. 6).

In addition to the general requirements outlined, the choice of laminated plates for the sectional capacitances was made on the basis of attaining low dielectric losses and high-RF-current-carrying capability combined with restrictive physical geometry, high-voltage operation, and proper capacitance value. No commercial or laboratory capacitors fulfilled these requirements as well as the laminated plates. The specific material finally selected was a 1/8-inch-thick teflon glass-cloth copper-clad laminate manufactured by the Polychem Division of the Budd Company under the trade number Di-Clad 522. This is a low and controlled dielectric-loss material which, for the frequencies being considered, has a relative dielectric constant of 2.6 and a dissipation factor less than 0.001. After being milled into 7-3/8 inch-square sheets, the material was photographically etched to leave a 3-7/8 inch-diameter copper-clad surface in the center of each side which served as the capacitor. A 1/16-inch strip of copper-clad material remaining between the center and one edge is used as a charging lead and for partial RF suppression.

The capacitances of the 74 final units were maintained within 0.5 pF by proper selection and careful preservation of tolerances. Extended DC voltage tests of the plates indicated that punch-through would not be experienced below 100 kV, and that creepage around the dielectric edges, even in an unpressurized environment, would not occur below 70 kV. The addition of the silicone rubber to the copper edges, for the purpose described in Sec. III-C, tended to increase the voltage where creepage-breakdown occurred as did, of course, immersion of the plates in a pressurized environment.

2. Gap Structures

In order to obtain a simple gap geometry, from a standpoint of fabrication, analysis, and electric-field considerations, a half-sphere structure was chosen. Several materials were investigated primarily with respect to their erosion rates and workability. A high melting point combined with a high coefficient of thermal conductivity, such as found in the silver- and copper-loaded tungsten materials, relate directly to low erosion rates. Nevertheless, since low duty-factor operation was envisioned in the experimental model, a hard aluminum alloy (No. 2017T4) with satisfactory characteristics was selected. In this material, it was possible to obtain 5/8-inch-diameter ball bearings which were subsequently machined to half-spheres.

3. Bonding

A procedure was required for accurately and efficiently bonding the aluminum gap structures to the copper-clad plates. Hot soldering was not feasible (even for materials other than aluminum) since the amount of heat required would tend to weaken the copper-dielectric bond, probably resulting in increased corona activity under high-voltage conditions. Furthermore, accurate positioning of the gap structure would be difficult. A search of bonding agents narrowed to a two-part low-resistance conductive cement manufactured by Emerson and Cuming, Incorporated as Eccobond Solder 56C. When properly cured at elevated temperatures, an extremely low-resistance relatively strong bond is obtained. A precision jig, as shown in Fig. 17, was constructed to allow repeatable and accurate bonding of the gap structures to the laminated plates. The procedure comprised positioning two cement-buttered gap structures in the jig, inserting the etched laminated plate, clamping the jig, and curing the assembly at 175°F for 10 minutes. Electrical resistance and mechanical strength of each bond were tested individually.
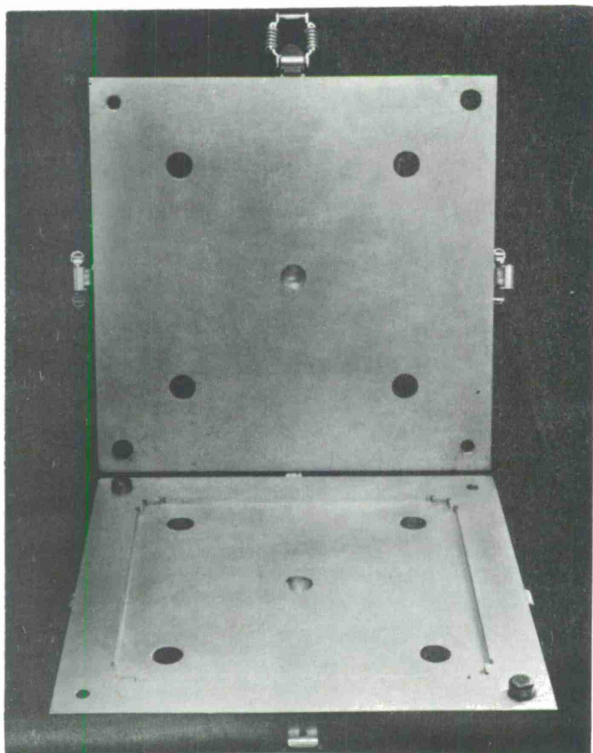
Fig. 17.   Precision bonding jig.

An unforeseen result of the oven cure was a slight increase in the warp and twist of the laminated plates. Additionally, a further factor was the reduced mechanical stability resulting from the removal, through etching, of a major portion of the copper-clad material. These factors combined to cause an excessive variability in gap spacing and, therefore, breakdown voltage. A total range in excess of ± 2 percent of the mean breakdown voltage was measured. In order to reduce this variation to acceptable levels, as explained in Sec. IV-A, a series of adjustable nylon screws and nuts was added to the edges of the plates. Succeeding measurements indicated that the variation in breakdown voltage had only been reduced to somewhat less than ± 2 percent. Although this represents only a small improvement, further adjustment was not practical.

4. Charging Resistors

The resistors used for charging the sectional capacitors must be large enough to limit the power supply follow-on current at the end of each pulse to allow gap de-ionization, yet small enough to permit rapid recharging of the capacitors for subsequent discharge. The only information available in the literature on de-ionization and re-ignition is furnished for specific gaps operating at DC. The successful extrapolation of these data to the high-frequency variable electrode and gas parameter situation seems improbable. Experimental determination, considering all probable electrode and gas parameters, indicated that a total charging resistance of 40 megohms permits consistent gap de-ionization and still allows charging times congruous with pulse-repetition frequencies of 50 pps. A varnished spiral carbon-film resistor was selected having a tested flashover of 75 kV, a power rating of 5W, and an end-to-end capacity of 0.2 pF. Two 20-M resistors charge each capacitor from a balanced power supply, resulting in a conservative application of ratings. The resistors, being fragile, chipped readily causing corona and thermal hot spots in the damaged area. Excessive care in handling was required to surmount this problem. The utilization of charging inductances was not considered due to the anticipated concurrent parasitic oscillations.

5. Radome

It is not desirable to pressurize gap structures individually because of size and triggering restrictions. Therefore, a low-loss RF container is necessary for pressurized operation of the transmitter. The combination of excellent electrical properties, high working pressures, full-access openings, and large overall size resulted in conflicting material and engineering requirements. Conventional solutions, suggested by several vendors, included combinations of Rexolite, fiberglass, and foam-filled fiberglass. Use of monolithic glass or ceramic materials was not practical. A satisfactory design, shown in Fig. 18, was finally evolved and constructed by Custom Materials, Incorporated. The radome cylinder wall and integral flanges were spun

Fig. 18. Pressurizable radome.

on a mandrel using 0.150-inch-thick polyester fiberglass. The top and bottom heads consist of a six-layer vacuum-pressed sandwich of polyester fiberglass, 1/4-inch cell honeycomb, and epoxy fiberglass clamped to the cylinder wall with 72 nylon screws and nuts. Large neoprene O-rings, positioned in grooves, aid in sealing the entire assembly. Pressure, power supply, and high-voltage RF connectors used in triggering are mounted in the heads. During initial pressure testing, the nylon bolts continually sheared and, eventually, one of the heads was also damaged. Tensile testing of the bolts indicated that they apparently possessed adequate ultimate strength and were superior to both a phenolic impregnated wood and a wrapped phenolic-glass fabric bolt which was also examined. Subsequent investigation disclosed that a bending moment caused by the deflection of the radome heads produced complex stresses in the bolts, resulting in failure. The problem was surmounted by increasing the head rigidity, by changing the form-factor of the bolt thread to help distribute stresses, and by using a larger (1-1/4 inch) bolt. This final design is capable of continuous safe operation to 50 psig. Calculations of the dielectric losses incurred in both the radome and the transmitter framework indicate that less than 0.1 percent of the incident power would be absorbed.

C. Ultraviolet-Triggering System

The most desirable method of triggering the multiple-transmitter gaps, as stated in Sec. III-B, would utilize applied overvoltage, ultraviolet, laser, or preferably a combination of these mechanisms. The practical realization of overvoltage triggering would involve very high-voltage multiple-triggering electrodes with their attendant distribution system and adjustment procedures in a unit already full of components and requiring multitudinous adjustments. Laser triggering, although promising effective results, is not well enough established to merit initial consideration. Therefore, ultraviolet triggering, along with the readily available self-breakdown through the application of slow overvoltage, will be the primary mechanisms utilized. Slow overvoltage triggering could be capable of producing satisfactory results since each gap that breaks down exposes the remaining gaps to increasing overvoltages, resulting in decreased transition times.

The ultraviolet-triggering system utilizes a spark as the primary ultraviolet-generating mechanism for reasons discussed in Sec. III-B. A conical reflector, positioned near the upper center of the transmitter, is used to distribute the radiation to the desired locations. An over-all representation of the system is shown in Fig. 19; a corresponding photograph of the equipment is presented in Fig. 20. Initial trigger energy stored at −20 kV in 32 ft of RG-214 is discharged into the center electrode of the three-ball gap by means of the coaxial thyratron switch. This unit consists of a 7620/HY10 ceramic thyratron housed in a coaxial impedance-transition structure, with the thyratron forming the center conductor. The −20-kV open-ended output present at the center electrode of the three-ball gap is a nominal 100-nsec pulse with an 8-nsec rise time as reproduced in Fig. 21(a). This rise time was obtained by increasing the thyratron reservoir voltage, by utilizing capacitive energy storage in the trigger circuit, and by operating inside the coaxial structure. The time delay of the output cable, as well as internal resistors, serve to isolate the three-ball gap from attendant reflections before breakdown.

Optimum operation of the three-ball gap, in a 50-psig air atmosphere, has been determined to occur for the case of all electrodes on-axis, an input-to-center electrode separation of 180 mils, and a center-to-output separation of 80 mils; all electrodes are fully adjustable. Although a theoretical decrease in response time could be obtained[28] by proper DC biasing of the
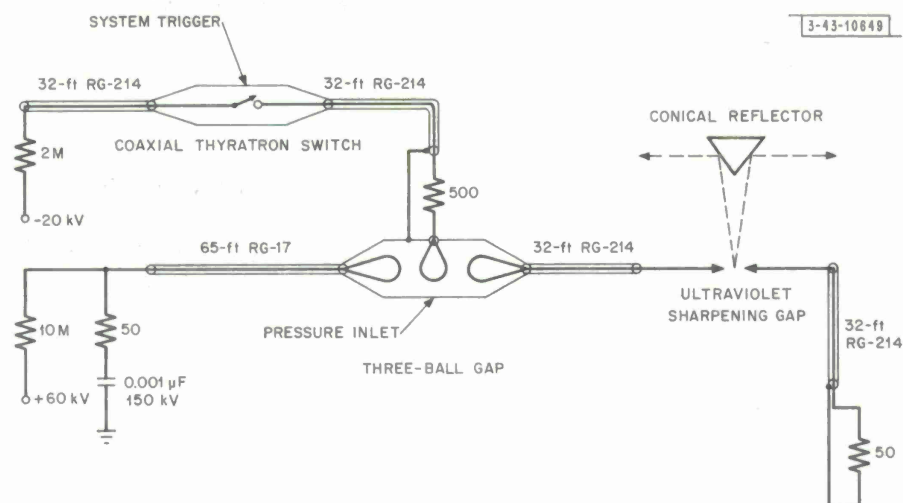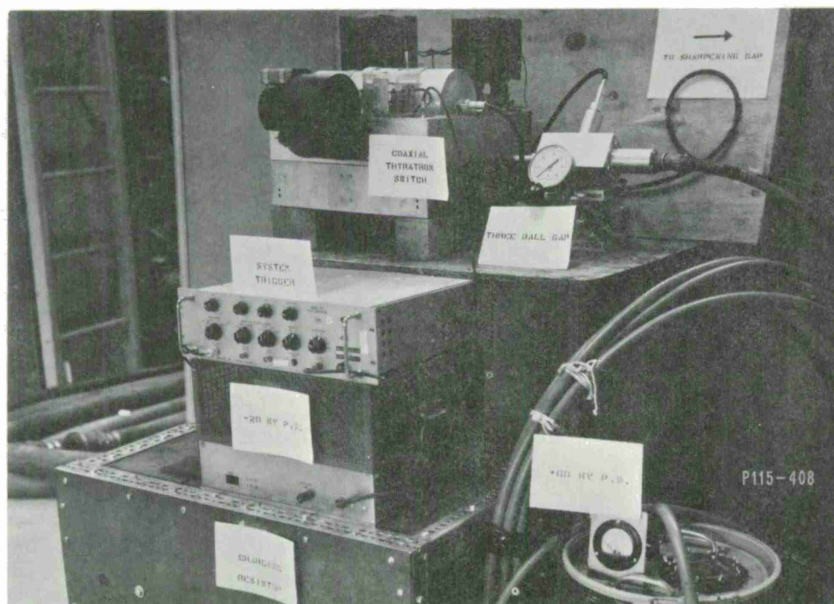
27

Fig. 19.   Ultraviolet triggering system.

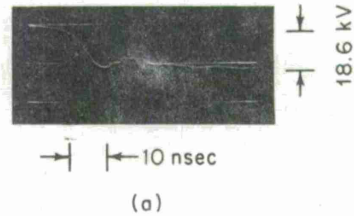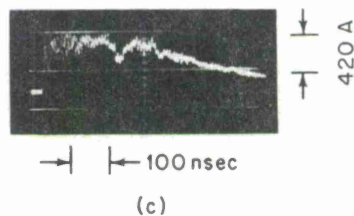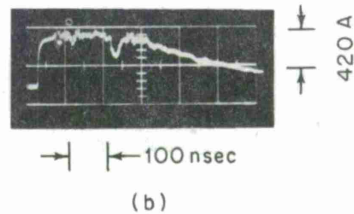Fig. 20.   Ultraviolet triggering equipment.

-43-10650

18.6 kV

→| |←10 nsec

(a)

Fig. 21. Ultraviolet system waveforms:
(a) coaxial thyratron switch output;
(b) three-ball gap output; (c) sharpening
gap output.

420 A

→| |←100 nsec

(b)

420 A

→| |←100 nsec

(c)

center electrode, the additional high-voltage complexity would probably negate any advantages obtained. Figure 21(b) is a photograph of the resultant output pulse utilizing a 65-ft RG-17 input cable charged to +60 kV. The apparent reflection-decay at the end of the pulse is caused by the RC matching network at the input of the charging line, which prevents high-voltage transients from damaging the line. Other operating modes, including the use of a 90-10 atmosphere or replacement of the center ball with a sharp needle, are also capable of producing satisfactory output pulses. As shown in the exploded view (Fig. 22), the three-ball gap makes full use of an

P115-422
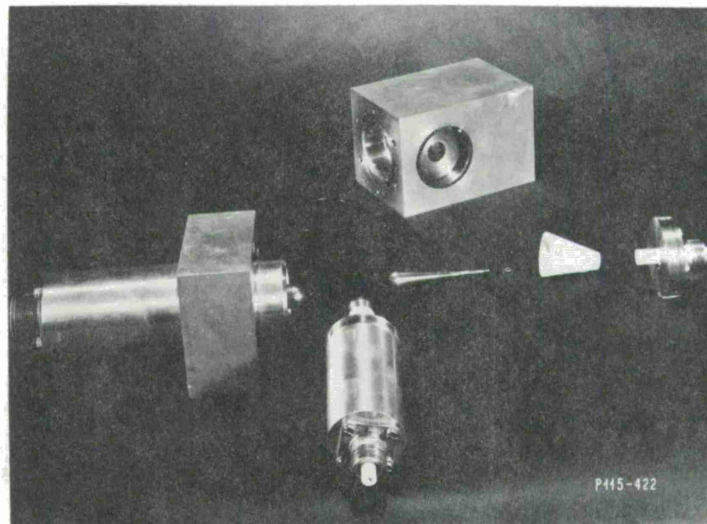
Fig. 22. Three-ball gap (exploded view).

impedance-matching coaxial structure to insure fast reflectionless pulse transfer. The electrodes are machined from a 26% Cu-74% W (by weight) sintered material manufactured by P. R. Mallory and Company as Elkonite 10W3. This and similar materials have been developed to carry high currents with good arc-resistance characteristics. The pulse emanating from the three-ball gap travels through 32 ft of RG-214 isolating line to the ultraviolet sharpening gap, which serves as the source of the ultraviolet radiation and can be seen in the lower center of Fig. 16. Without the isolating line, internal reflections would interfere with the arc-formation processes. Finally, the pulse is either terminated by a matched load or a short circuit. Although the short circuit causes multiple reflections, the discharge ionization current (and therefore ultraviolet intensity) is almost doubled. The sharpened terminated pulse, a photograph of which is reproduced in Fig. 21(c), has a rise time of about 2 nsec; the unsharpened pulse rise time is 10 nsec. This improvement occurs because the ultraviolet sharpening gap, which is adjusted for a 3/64-inch spacing, is considerably overvolted, producing fast transition times. High-voltage RF connectors were either laboratory constructed or extensively modified commercial connectors. Considerable difficulty was encountered with either type.

The conical reflector consists of a 3-1/2 inch-diameter optically polished aluminum surface coated with magnesium fluoride, and reflects essentially all the radiation impinging on it in the primary region of interest. The aluminum surface was originated by plotting various shapes to obtain maximum illumination of all transmitter gaps allowing for variations in mechanical tolerances. Figure 23 is a photograph of the assembled transmitter and shows the reflector mounted in the top head.
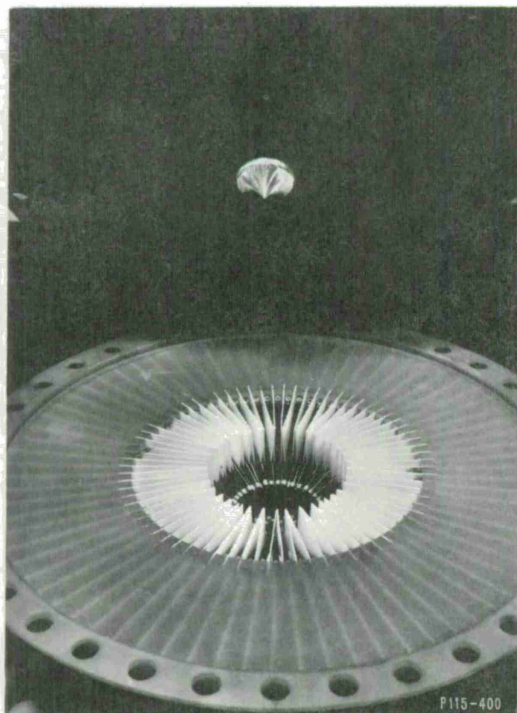

Fig. 23. Assembled transmitter.

The ultraviolet system, as described, delivers an integrated pulse energy in excess of 5 J, and a terminated peak current of 600 A, when operating from a 60-kV power-supply voltage. Although a pulse of several hundred nanoseconds is obtained, the peak ultraviolet intensity during

the first few nanoseconds determines the triggering response. It is clear from the discussion in Sec. III-C that the present system is perhaps five or ten orders of magnitude below desirable peak intensity levels. An increase in power-supply voltage to at least 300 kV would increase the intensity to a useful level but certainly could not be accomplished without a redesigned integrated system not using high-voltage RF connectors. Similarly, reducing impedance levels by a factor of five would require cable diameters four times larger than presently used, assuming constant voltage and dielectric conditions, as well as involving redesigned connectors and gaps. A slight increase in peak intensity could be obtained most readily by altering the electrode materials and geometry of the ultraviolet sharpening gap and modifying the conical reflector to obtain sharper focusing. Realistically, a new ultraviolet system incorporating all these factors, or entirely different concepts, is probably required.

D.   Test Range

Field testing of the completed transmitter was performed at the Lincoln Laboratory Antenna Test Range[35] where ground-level range paths have been graded to within ±1 inch of a true plane. Thus, measurements of the far-field radiation characteristics of the transmitter could be made, utilizing and controlling the ground reflections, simulating free-space conditions. The transmitter and receiving antenna, separated by 600 ft, were placed on towers approximately 33 ft above the mean ground plane. The upper section of the transmitter tower is nonmetallic. A photograph of the transmitter tower, looking back toward the receiving antenna, is reproduced in Fig. 24. A wide-band half-wave dipole, connected directly to a Tektronix 519 oscilloscope, provided the desired transmitter waveforms. All measurements made use of the radar equation since direct transmitter interconnection is not possible. System calibration was accomplished by replacing the magnetic dipole transmitter with a CW test transmitter.
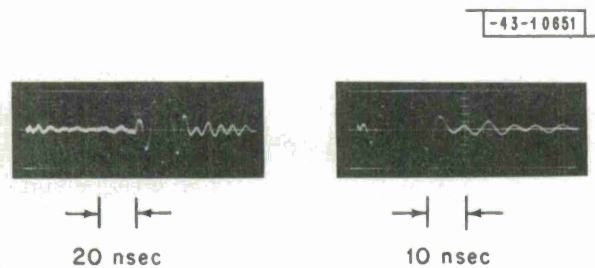

Fig. 24.   Test range.

20 nsec   10 nsec

Fig. 25.   Transmitter output waveforms.

CONDITIONS:
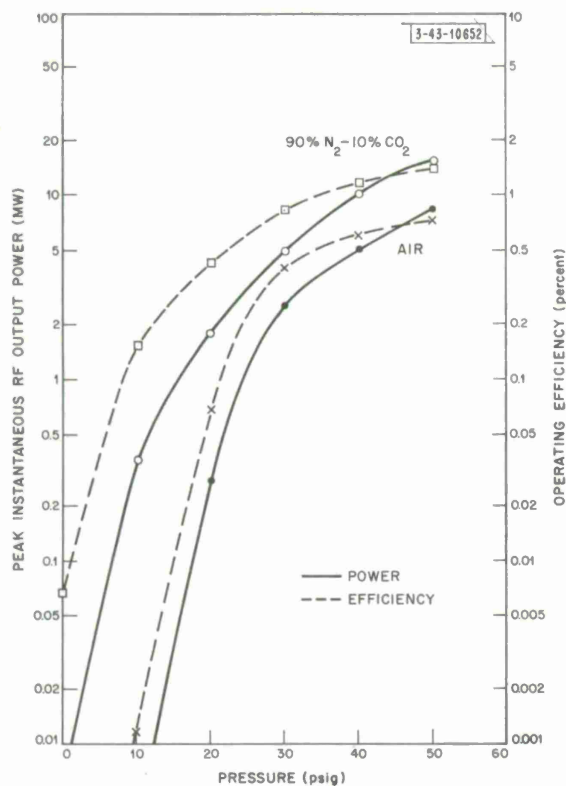50 psig 90% N_2-10% CO_2
ULTRAVIOLET TRIGGERED

Fig. 26.   Transmitter output parameters
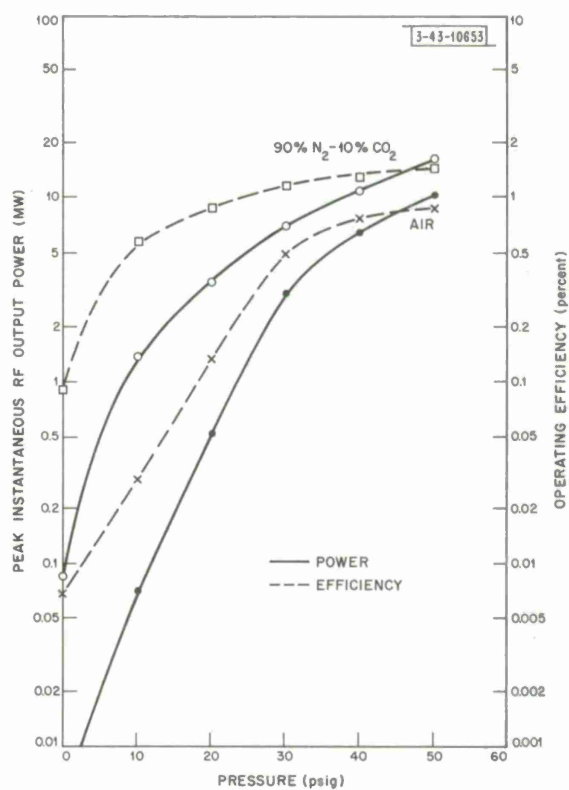for self-breakdown operation.

Fig. 27.   Transmitter output parameters
for ultraviolet-triggered operation.

E. Initial Transmitter Tests

In order to establish whether mechanisms other than gap synchronization would limit trans-
mitter performance operation with a single gap when all others were short-circuited, a test
was attempted. This initial test, performed without pressurization, produced anomalous radi-
ation patterns and negligible output power. Subsequent reflection on this problem revealed that
the defect was in the simulation, especially the timing aspect, of gap performance. In effect,
the transmitter was forced to operate in a nonsynchronous mode. A comparison of the result-
ant radiation pattern with a computer simulation verified this phenomenon.

Initial operation of the transmitter in the normal mode was also unsuccessful using all com-
binations of triggering, pressurization, and gas type. Subsequent internal examination of the
transmitter revealed a dislocated ball gap and evidence of arcing between the output ends of the
charging resistors. This arcing was precipitated by the missing ball gap; the resistor ends
are normally at equal potentials. In addition to repairing the dislocated ball gap, teflon spacers
were inserted between the resistors as a precaution.

F. Transmitter Evaluation

The modified transmitter was operated at the test range under self-breakdown and ultraviolet-
triggered conditions using all combinations of gas type and pressure. Figure 25 is a photograph
of representative transmitter waveforms received by the test antenna and displayed directly on
the oscilloscope. Transmitter operating parameters were determined from a series of such
photographs, each representing a single output pulse. A measured operating frequency of
130 MHz and a pulse width (to 10-percent power) of 22 nsec agree with the experimental design
and the pressure-vessel data indicating total losses approximating the radiation resistance.
Furthermore, as expected, these parameters are not a function of gas or triggering conditions.
Figure 26 is a plot of transmitter output power and operating efficiency for self-breakdown op-
eration. Reproducibility of data was poor at the lower pressures, but relatively consistent at
higher pressures (particularly for the 90-10 mixture). This is attributed to the nonsynchroniza-
tion of gap breakdown at the lower pressures and could be observed as a series of small random
discharges stretched over hundreds of nanoseconds. Ultraviolet-triggered operation improved
the low-pressure output by an order of magnitude, as shown in Fig. 27. High-pressure operation
was not significantly affected and the peak-instantaneous output power obtained with 50 psig of
90-10 mixture was 16.2 MW compared with 15.8 MW utilizing self-breakdown. The efficiency
appears to have reached a limit near 1.5 percent, regardless of further increases in pressure.
The lack of adequate ultraviolet intensity, as discussed in Sec. III-C, is believed to be primarily
responsible for this effect. Additionally, increasing pressures result in higher gas densities,
which further attenuate the ultraviolet intensity. Ultraviolet triggering is somewhat erratic
even with 50-psig pressurization; transmitter discharge does not occur for every ultraviolet
burst. This lack of ultraviolet intensity caused large variation in gap formative times and slow-
gap transition times, resulting in poor multiple-gap synchronization. Gap losses, charge re-
distribution, and other effects are believed to be of secondary importance in limiting transmitter
operating efficiency.

The horizontal radiation pattern was verified to be that of a magnetic dipole by rotating the
transmitter in 10° increments. Multiple-pulse operation was attempted by triggering the trans-
mitter at rates up to 50 pps. Because of the inadequacies of the ultraviolet system, erratic

33

operation, including missing pulses, occurred. Although increasing the operating voltage resulted in more reliable triggering, interpulse self-breakdown was encountered. A satisfactory intermediate operating point could not be established.

V. CONCLUSIONS AND RECOMMENDATIONS

The data obtained on the magnetic dipole transmitter indicate that spark-transmitter operation at VHF and lower frequencies is feasible. Furthermore, such devices need not be limited to the ring structure investigated in this program. It is probable that transmitter efficiency is limited primarily by lack of synchronization, and secondarily by spark-gap losses, charge redistribution, and other related effects. A detailed examination of the elementary unit oscillator and its synchronization possibilities might disclose basic phenomena that are not now readily apparent. Additionally, substantial experimental work is still required in all areas of spark-gap phenomena. Although ultraviolet triggering produced higher transmitter efficiencies than the self-breakdown mode, it merits further investigation only if used in conjunction with other triggering modes or if larger peak intensities can be obtained. Use of a laser, overvoltage, or combination mode is recommended in future applications. Overvoltage triggering, although the most positive mechanism, requires an elaborate high-voltage trigger-distribution system which must be electrically isolated from the main RF output. In order to realize optimum transmitter performance with any triggering system, it is still important to utilize identical close-tolerance spark gaps. This implies the development of a simple and reliable means of gap adjustment. The advantages of pressurizing the spark gaps with 30 to 50 psig of a $90\% N_2 - 10\% CO_2$ atmosphere have been clearly demonstrated. Although the use of dielectric-liquid gaps, or other novel switching devices, does not appear practical at this time, a parallel investigation of such concepts may prove valuable in future applications.

REFERENCES

1. K. Landecker and K. S. Imrie, "A Novel Type of High Power Pulse Transmitter," Australian J. Phys. 13, No. 4, 638 (1960).

2. L. T. Dolphin, Jr., A. F. Wickersham, Jr., and F. E. Firth, "The Investigation of the Application of Modern Spark Gap Techniques to High-Power Transmitter Design," Technical Summary Report 1, Contract Nonr-4178(00), ARPA Order No. 463, SRI Project 4548, Stanford Research Institute, Menlo Park, California (January 1964).

3. L. T. Dolphin, Jr. and A. F. Wickersham, Jr., "An Investigation of the Application of Modern Spark Gap Techniques to High-Power Transmitter Design," Technical Summary Report 2, Contract Nonr-4178(00), ARPA Order No. 463, SRI Project 4548, Stanford Research Institute, Menlo Park, California (June 1964).

4. _____, "Modern Spark Transmitter Techniques," Final Report, Contract Nonr-4178(00), ARPA Order No. 463, SRI Project 4548, Stanford Research Institute, Menlo Park, California (December 1964).

5. _____, "The Generation of Megawatt Peak Powers by Modern Spark-Transmitter Techniques," Final Report, Contract Nonr-4178(00), ARPA Order No. 463, SRI Project 4548, Stanford Research Institute, Menlo Park, California (February 1966).

6. L. T. Dolphin, Jr. and F. E. Firth, "Spark Transmitter Techniques for EM Pulse Generation," Technical Summary Report 4, Contract Nonr-4178(00), ARPA Order No. 463, SRI Project 4548, Stanford Research Institute, Menlo Park, California (August 1966).

7. L. T. Dolphin, Jr., F. E. Firth, and A. F. Wickersham, Jr., "RF Power Generation by Spark-Gap Switching Techniques," Quarterly Technical Progress Report 1, Contract AF 30(602)-4266, ARPA Order No. 843, SRI Project 6000, Stanford Research Institute, Menlo Park, California (September 1966).

8. S. A. Schelkunoff and H. T. Friis, Antennas: Theory and Practice (Wiley, New York, 1952), p. 503.

9. J. D. Kraus, Antennas (McGraw-Hill, New York, 1950), p. 164.

10. A. Papoulis, The Fourier Integral and Its Applications (McGraw-Hill, New York, 1962), p. 28.

11. D. F. McDonald and S. J. Brient, "Nanosecond Pulse Breakdown Initiation and Growth," Final Technical Documentary Report No. RADC-TDR-63-525, BDM Project No. 4506, Task No. 450603, Braddock, Dunn and McDonald, Inc., El Paso, Texas (January 1964).

12. "Nanosecond R. F. Pulse Breakdown Study," Technical Documentary Report No. RADC-TDR-64-204, Microwave Associates, Inc., Burlington, Massachusetts (July 1964).

13. J. M. Meek and J. D. Craggs, Electrical Breakdown of Gases (Oxford University Press, London, 1953), pp. 348 − 373.

14. Ibid., pp. 252 − 290.

15. R. C. Fletcher, "Impulse Breakdown in the 10^{-9}-Second Range of Air at Atmospheric Pressure," Phys. Rev. 76, No. 10, 1501 (1949).

16. J. M. Proud and P. Felsenthal, "Nanosecond Breakdown in Gases," Final Technical Documentary Report No. RADC-TDR-62-617, Space Sciences, Inc., Natick, Massachusetts (December 1962).

17. P. Felsenthal and J. M. Proud, "Nanosecond Pulse Breakdown in Gases," Final Technical Documentary Report No. RADC-TDR-64-38, Space Sciences, Inc., Waltham, Massachusetts (March 1964).

18. _____, "Nanosecond Pulse Breakdown in Gases," Phys. Rev. 139, No. 6A, 1796 (1965).

19. F. R. Dickey, Jr., "Contribution to the Theory of Impulse Breakdown," J. Appl. Phys. 23, No. 12, 1336 (1952).

20. P. Felsenthal, Space Sciences, Inc., Waltham, Massachusetts, private communication.

21. B. J. Elliott, "On the Generation of Intense Fast-Rising Magnetic Field Pulses," M. L. Report No. 1095, Microwave Laboratory, W. W. Hansen Laboratories of Physics, Stanford University, Stanford, California (October 1963).

22. J. D. Cobine, Gaseous Conductors: Theory and Engineering Applications (Dover Publications, New York, 1958), p. 345.

23. J. Fischer and G. T. Zorn, "Reduction of Delay Between Particle Passage and Spark Chamber Spark," IRE Trans. Nucl. Sci. NS-9, No. 3, 261 (1962).

24. L. T. Dolphin, Jr., F. E. Firth, and A. F. Wickersham, Jr., "RF Power Generation by Spark-Gap Switching Techniques," Quarterly Technical Progress Report 1, Contract AF 30(602)-4266, ARPA Order No. 843, SRI Project 6000, Stanford Research Institute, Menlo Park, California (September 1966).

25. D. H. Wilkinson, Ionization Chambers and Counters (Cambridge University Press, London, 1950).

26. G. Schrank and G. Henry, "Spark-Gap Trigger System," Rev. Sci. Instr. 35, No. 10, 1326 (1964).

27. T. J. Williams, "The Theory and Design of the Triggered Spark Gap," Technical Memorandum 186-59-(14), Sandia Corporation, Albuquerque, New Mexico (May 1959).

28. J. H. Adlam and L. S. Holmes, "Production of Millimicrosecond Current Pulses Using a Pressurized Spark Gap," J. Sci. Instr. 37, 385 (1960).

29. A. Gold and H. B. Bebb, "Theory of Multiphoton Ionization," Phys. Rev. Letters 14, No. 3, 60 (1965).

30. G. L. Weissler in Handbuch der Physik, Vol. 21 (Springer-Verlag, Berlin, 1956), pp. 326 − 329.

31. "Development of an Ultrafast Moderate Energy Pulse Power System," Technical Report No. AFWL-TR-65-1, Field Emission Corporation, McMinnville, Oregon (January 1966).

32. T. F. Godlove, "Nanosecond Triggering of Air Gaps with Intense Ultraviolet Light," J. Appl. Phys. 32, No. 8, 1589 (1961).

33. F. M. Collins, "Design Study of a Photoelectrical Trigger System," Technical Report No. AFWL-TR-65-157, Field Emission Corporation, McMinnville, Oregon (December 1965).

34. W. K. Pendleton and A. H. Guenther, "Investigation of a Laser Triggered Spark Gap," Rev. Sci. Instr. 36, No. 11, 1546 (1965).

35. A. Cohen and A. W. Maltese, "The Lincoln Laboratory Antenna Test Range," Microwave J. 4, No. 4, 57 (1961).

DOCUMENT CONTROL DATA – R&D

(Security classification of title, body of abstract and indexing annotation must be entered when the overall report is classified)

1. ORIGINATING ACTIVITY *(Corporate author)*	2a. REPORT SECURITY CLASSIFICATION
Lincoln Laboratory, M.I.T.	Unclassified
	2b. GROUP
	None

3. REPORT TITLE

Project MAPOLE (Magnetic Dipole Spark Transmitter)

4. DESCRIPTIVE NOTES *(Type of report and inclusive dates)*

Technical Note

5. AUTHOR(S) *(Last name, first name, initial)*

Fraser, Marcel P.

6. REPORT DATE	7a. TOTAL NO. OF PAGES	7b. NO. OF REFS
22 May 1967	44	35

8a. CONTRACT OR GRANT NO.	9a. ORIGINATOR'S REPORT NUMBER(S)
AF 19 (628)-5167	
b. PROJECT NO.	Technical Note 1967-24
627A	
c.	9b. OTHER REPORT NO(S) *(Any other numbers that may be assigned this report)*
d.	ESD-TR-67-265

10. AVAILABILITY/LIMITATION NOTICES

Distribution of this document is unlimited.

11. SUPPLEMENTARY NOTES	12. SPONSORING MILITARY ACTIVITY
None	Air Force Systems Command, USAF

13. ABSTRACT

This report describes theoretical and experimental work on the development of a VHF high-power closed-ring spark transmitter, a device theoretically capable of producing gigawatt peak powers in the nanosecond pulse-length region. The investigation and this report were conveniently divided into three distinct, though interrelated, categories: First, the theoretical aspects of transmitter performance; second, an investigation of certain aspects of spark-gap performance germane to the entire undertaking; finally, the construction and experimental evaluation of the complete transmitter.

14. KEY WORDS

spark transmitter	high-RF power	ultraviolet triggering
magnetic dipole	spark gap	VHF